Applied Catalysis B: Environmental 328 (2023) 122511

Contents lists available at ScienceDirect

Applied Catalysis B: Environmental

journal homepage: www.elsevier.com/locate/apcatb

Activation of peroxymonosulfate by La_2CuO_4 perovskite for synergistic removal of *Microcystis aeruginosa* and microcystin-LR in harmful algal bloom impacted water

Panpan Gao [a,b,c], Yunyi He [a], Shihuan Lu [a], Mengfan He [a], Zhiqun Liu [a], Yang Deng [d], Zhiquan Liu [a,b,c], Ting Xu [e], Hangjun Zhang [a,b,c,*]

[a] School of Life and Environmental Sciences, Hangzhou Normal University, 311121 Hangzhou, Zhejiang, China
[b] School of Engineering, Hangzhou Normal University, 311121 Hangzhou, Zhejiang, China
[c] Zhejiang Provincial Key Laboratory of Urban Wetlands and Regional Change, 311121 Hangzhou, Zhejiang, China
[d] Department of Earth and Environmental Studies, Montclair State University, Montclair, NJ 07043, USA
[e] Zhejiang June5 Environment Co., Ltd, Hangzhou, Zhejiang, China

ARTICLE INFO

Keywords:
Microcystis aeruginosa
Peroxymonosulfate
La_2CuO_4 perovskite
Algal organic matters
Microcystin-LR

ABSTRACT

The cyanobacterial blooms induced water safety problems have attracted tremendous concerns due to the adverse influences on aqueous ecosystem and human health. This study developed a novel perovskite-type catalyst for heterogeneous peroxymonosulfate (PMS) activation as an emergency measure to remove harmful algae. The results indicated that significant removal efficiency of *Microcystis aeruginosa* cells (97%) and chlorophyll-a (100%) was achieved within 20 min in La_2CuO_4/PMS system without significant release of dissolved organic carbon and metals in water. $^{\bullet}OH$, $SO_4^{\bullet-}$, $^1O_2$ and $^{\bullet}O_2^-$ generated were all responsible for algae inactivation and subsequent algal organic matters removal. Moreover, the heterogeneous catalytic mechanism was proposed that La portion in La_2CuO_4 favored the cells destabilization by increasing zeta potential of algae suspension, while variable Cu portion facilitated the electron transfer to improve the yields of $^{\bullet}OH$ and $SO_4^{\bullet-}$. This study demonstrates that the new catalytic PMS process promises viable and effective control of harmful algal bloom impacts in water treatment.

1. Introduction

Harmful algal blooms (HABs), which is primarily driven by nutrient over-enrichment and aggravated by a changing climate, is viewed as a global threat to the safety and security of drinking water supply [1]. *Microcystis aeruginosa* (*M. aeruginosa*) is widely acknowledged to be the prevailing cyanobacterial species in the eutrophic water, producing profound impacts, such as aesthetic problems, problematic taste and odor-causing matters, as well as the release of algal toxins. In particular, among harmful algal organic matters (AOM), microcystin-LR (MC-LR) is a representative toxic microcystins (MCs) due to the strong hepatotoxicity with a maximum acceptable concentration of 1.0 μg/L in the World Health Organization (WHO) drinking water standards [2]. Another concern is that the unwelcome AOM released serve as potential precursors of disinfection by-products (DBPs) during subsequent water disinfection [3], posing risks to human health. Therefore, the development of viable and effective treatment processes for addressing the HABs impacts is urgently needed.

Different treatment technologies have been explored, but conventional biological treatment (e.g., aquatic plants, allelopathy of phytoplankton), filtration (e.g., mechanical salvage, membrane filtration) and chemical technologies (e.g., $CuSO_4$, $KMnO_4$) have been restricted by diverse limitations, such as long retention duration, low removal efficiency and the formation of secondary pollution due to the high mobility, steric effects and powerful electrostatic repulsion of algae cells [4–7]. Additionally, algal metabolites challenge the coagulation-sedimentation-filtration treatment train at conventional drinking water treatment plants (DWTPs) [8].

Recently, sulfate radical-based advanced oxidation processes (SR-AOPs) have emerged as a state-of-the-art water treatment technology for decomposing or mineralizing refractory toxic organic contaminants and inactivating pathogens in environmental remediation by taking leverage

* Corresponding author at: College of Life and Environmental Sciences, Hangzhou Normal University, 311121 Hangzhou, Zhejiang, China.
E-mail address: 13819172516@163.com (H. Zhang).

https://doi.org/10.1016/j.apcatb.2023.122511
Received 15 December 2022; Received in revised form 3 February 2023; Accepted 20 February 2023
Available online 26 February 2023

of highly reactive oxygen species (ROS, e.g. $SO_4^{\bullet-}$, $^{\bullet}OH$, $^{\bullet}O_2^-$ and $^1O_2$) [9–13]. Commonly, peroxymonosulfate (PMS, HSO_5^-) is preferable in SR-AOPs in comparison with peroxydisulfate (PDS, $S_2O_8^{2-}$) due to the unsymmetrical chemical structure, higher cost effectiveness and more activation approaches [14]. As such, PMS combined with Fe(II) or light irradiation have been widely used to pre-oxidize *M. aeruginosa* for improving coagulation and alleviating membrane fouling [15,16]. However, homogeneous catalytic processes suffer from metal ions at high concentrations and difficulties in recovering the catalyst. In contrast, the $SO_4^{\bullet-}$-based heterogeneous catalytic technologies have received enormous attention for algae inactivation. Fan et al. constructed multiple heterogeneous photocatalysts such as $ZnFe_2O_4/Ag_3PO_4/g\text{-}C_3N_4$ and $Ag_2O/g\text{-}C_3N_4$ for the inactivation of *M. aeruginosa* and degradation of MC-LR under the visible light irradiation [17,18]. Nonetheless, photocatalytic activation is limited by prolonged reaction time and low light utilization. Of interest, very little attention to persulfate based heterogeneous catalyst has been paid for the control of cyanobacterial blooms.

Perovskite oxides families (ABO_3 or A_2BO_4) as the emerging functional nanomaterials have been widely probed in the field of solar energy, sensors, electrochemistry and catalytic oxidation, due to the high design flexibility, controllable defects to create ionic or electronic conductivities, tunable surface property, and stability [19–22]. In their compositions, A is an alkaline-earth or rare-earth element, while B is a transition metal element. The unique structural, physicochemical and electronic properties can be readily tailored by regulating chemical species and composition [23,24]. Yan et al. reported Ag/AgCl modified $LaFeO_3$ as a perovskite-type photocatalyst for HABs control, where the produced $^{\bullet}O_2^-$ and $^{\bullet}OH$ could effectively change the permeability of algae cells membrane and destroy the photosynthesis and antioxidant systems of *M. aeruginosa* [25]. Our previous works also demonstrated several La-based perovskites for remarkable degradation of various antibiotics and illustrated an oxygen vacancies dependent PMS activation mechanism, where $LaCoO_3$ presented the highest activity followed by La_2CuO_4, $LaMnO_3$ and then $LaFeO_3$ [23,26,27]. Yet there are few studies on perovskite-type catalysts activated PMS heterogeneous system for removal of harmful algae. Considering the widespread utilization of $CuSO_4$ as excellent algaecide and toxic nature of cobalt ions to human beings and the ecosystem [21], the construction of heterogeneous Cu-based perovskite is a plausible PMS catalyst for surmounting the HAB-impacted water issues.

This study aimed to synthesize La_2CuO_4 perovskite for activation of PMS to remove *M. aeruginosa* and degrade microcystins in water. The electron-rich transition metal in La_2CuO_4 would serve as donor to drive PMS decomposition and ROS generation, while the immigration of oxygen vacancies in the surface layer might be favorable for the high charge conductivity [19]. Specific objectives of this study include to: 1) evaluate the effects of La_2CuO_4/PMS dosage, stirring speed, solution pH and different realistic water matrixes on the catalytic removal efficiency; 2) elucidate the heterogeneous catalytic mechanisms by identifying ROS, investigating their contributions to algae inactivation, recognizing the roles of crucial active ingredients in the La_2CuO_4 perovskite and density functional theory (DFT) calculation; and, 3) determine the toxin release and propose the plausible MC-LR degradation pathways in the La_2CuO_4/PMS system. Results provide scientific basis for assessment of technical performance and mechanisms of the new catalytic oxidation process.

2. Materials and methods

2.1. Chemicals and reagents

All the chemicals were used as received from commercial suppliers without further purification. Trihydrate copper nitrate ($Cu(NO_3)_2\bullet 3H_2O$, 99%), anhydrous ethanol (99%), methanol (MeOH, 99%), *tert*-butanol (TBA, 99%), furfuryl alcohol (FFA, 99%), isopropanol (IPA, 99%), and *p*-benzoquinone (BQ, 99%) were purchased from Sinopharm Chemical Reagent Co., Ltd. Peroxymonosulfate (PMS, OXONE@, $KHSO_5\bullet 0.5KHSO_4\bullet 0.5K_2SO_4$), hexahydrate lanthanum nitrate ($La(NO_3)_3\bullet 6H_2O$, 99%), potassium hydroxide (KOH, 95%), glycine (99%) were obtained from Aladdin. 5,5-Dimethyl-1-pyrroline (DMPO, 99%) and 2,2,6,6-tetramethyl-4-piperidinol (TEMP, 99%) for EPR-spectroscopy were purchased from Sigma-Aldrich. Methanol (LC/MS grade, USA) and acetonitrile (LC/MS grade, USA) were provided from Thermo Fisher Chemical. Deionized water (18.25 cm•Ω) was used throughout this study.

2.2. Synthesis and characterizations of La_2CuO_4 perovskite

The La_2CuO_4 perovskite was synthesized using a modified hydrothermal-calcination method [24]. In a typical run, 3 mmol $La(NO_3)_3\bullet 6H_2O$ and 3 mmol $Cu(NO_3)_2\bullet 3H_2O$ were dissolved in 40 mL deionized water. Then, 20 mL 0.5 M KOH was added dropwise into the aforementioned solution under a magnetic stirring. After 2-hr mixing at room temperature for completion of the precipitation reaction, 0.06 g glycine was added. The obtained mixture was subsequently transferred into a 100 mL Teflon autoclave, and then heated in an oven at 180 °C for 12 h. After a natural cooling to room temperature, the collected precipitates were rinsed three times with deionized water and anhydrous ethanol, and then dried at 60 °C overnight. Finally, the dried precipitate was ground and calcined in a muffle furnace in air at 700 °C for 5 h with the heating ramp of 5 °C/min to obtain La_2CuO_4 perovskite. Pure La_2O_3 and CuO catalysts were also synthesized at the identical conditions except for the absence of $Cu(NO_3)_2\bullet 3H_2O$ or $La(NO_3)_3\bullet 6H_2O$, respectively.

Various characterization techniques were used to analyze the synthesized catalysts, including powder X-ray diffractometer (XRD), field emission scanning electron microscopy (FE-SEM), Brunauer-Emmett-Teller (BET), X-ray photoelectron spectrometer (XPS), and Fourier transform infrared spectroscopy (FTIR). Details of the experiments are shown in Text S1.

2.3. Experimental procedures

2.3.1. Cultivation of *M. aeruginosa*

M. aeruginosa FACHB 905 was purchased from the Institute of Hydrobiology, Chinese Academy of Science, and cultured with BG-11 medium (Table S1) in an intelligent artificial climate incubator (HP1500GS, Wuhan Ruihua Instrument & Equipment Co., Ltd). The light intensity was 3000 1ux light at a constant temperature of 25 ± 1 °C with a 14 h light and 10 h dark cycle. *M. aeruginosa* cells at a steady state were harvested and centrifuged at 4000 rpm for 10 min. The supernatant was removed from the centrifuge tube to remove the culture medium, before algae precipitated was diluted by deionized water for further experiments. In this study, the initial density of *M. aeruginosa* was approximately $(2.5 \pm 0.5) \times 10^6$ cells/mL, which was measured by the absorbance at 680 nm of UV–visible spectrophotometer (OD_{680} = 0.28). The initial pH of algae solution was adjusted to 7.0 by 0.1 mM NaOH or 0.1 mM HNO_3.

2.3.2. *M. aeruginosa* removal experiments

Algae removal experiments were conducted with 100 mL of simulated *M. aeruginosa*-laden suspension in a 150 mL glass beaker at room temperature of (25 ± 1) °C. The La_2CuO_4 catalyst was first added into the algal suspension followed addition of the PMS stock solution to launch the catalytic reaction. To simulate the coagulation process in drinking water treatment plants, the algal suspension was rapidly stirred at 250 rpm for 5 min followed by another 5-min mixing at 40 rpm, and 10-min settling. At given time intervals, aliquots of supernatant samples were withdrawn from 2 cm below the water surface, and immediately mixed with 100 μL methanol to quench any residual reactive radicals and terminate any possible further oxidation. To evaluate the effects of

La_2CuO_4 and PMS dosage, two sets of batch treatment experiments were carried out. In the first set, the La_2CuO_4 concentration was varied at 75, 150, 225, 300, 375, 450 mg/L with a fixed PMS dose at 0.24 mM. In the other group, the PMS dose ranged from 0.16, 0.19, 0.24, 0.32, 0.48, to 0.96 mM, while La_2CuO_4 was fixed at 300 mg/L. Meanwhile, the control groups were conducted at the same conditions without the addition of La_2CuO_4 or PMS. PMS concentration was quantified using a spectrophotometric method based on a modified iodometric titration (Text S2) [23]. In order to study the effect of different water matrix, the algae precipitated was diluted by Xixi Wetland lake water and tap water to ensure the initial density of algae of $(2.5 \pm 0.5) \times 10^6$ cells/mL, respectively. All the treatment experiments were conducted in triplicates. Data shown in figures represent the average of these measurements with error bars representing one standard deviation.

2.4. Analytic methods

2.4.1. Removal efficiency of M. Aeruginosa

M. Aeruginosa cells were counted with a hemocytometer plate under the microscope (Nikon Eclipse E100, Japan). The removal efficiency (Re) of *M. Aeruginosa* is calculated as follows:

$$Re = (C_0 - C_t)/C_0$$

Where C_0 and C_t are the *M. Aeruginosa* cell concentrations in the control and treatment samples at t min, respectively. The *M. aeruginosa* cell concentration is also positively correlated with the chlorophyll-a (Chl-a) content. Determination of Chl-a removal efficiency is provided in detail in Text S3.

2.4.2. Analysis of metals and DOC release

The algal suspension was centrifuged at 8000 rpm for 10 min. Then the supernatant sample was filtered through a 0.45 μm membrane for analyses of released metals cations and dissolved organic carbon (DOC). Since K^+, Ca^{2+} and Mg^{2+} are the key elements in the cells membrane of *M. aeruginosa*, their release indirectly indicates the integrity of *M. aeruginosa* cells membrane in the La_2CuO_4/PMS system. Residual Cu^{2+} in solution was also measured to assess the stability of the La_2CuO_4 catalyst. An inductively coupled plasma optical emission spectrometer (ICP-OES, iCAP 7400, Thermo Scientific, USA) and a TOC/TN analyzer (TOC-LCPH CN200, Shimadzu, Japan) were used to measure the concentrations of residual metals and DOC in water, respectively.

Three-dimensional fluorescence excitation emission matrixes (3D-EEMs) spectroscopy (F-4600, Hitach, Japan) was used to observe the variations of AOM, including extracellular organic matter (EOM) and intracellular organic matter (IOM). The detailed pretreatment procedures are present in Text S4.

2.4.3. Observation of algae cells morphology

The *M. aeruginosa* suspension was centrifuged at 8000 rpm for 10 min before the supernatant was discarded. The collected algae samples were mixed with 2.5% glutaraldehyde for 4 h, and then rinsed using a phosphate buffer solution for 15 min. The rinsing was repeated three times. Subsequently, the algae cells were dehydrated using different concentrations of ethanol (30%, 50%, 70%, 80%, 90%, and 100%) for 10 min each with gentle agitation. The dehydrated *M. aeruginosa* cells were dried by a vacuum freeze dryer and mounted on a copper stub to coat with gold for further SEM analysis.

2.4.4. Analysis of MC-LR

Extracellular MC-LR concentrations in the supernatant samples were measured with selective solid-phase extraction (SPE) and ultra-performance liquid chromatography in combination with triple quadrupole mass spectrometry (UPLC-MS/MS, I-Class-Xevo TQ-S Micro, Waters, USA). Meanwhile, the MC-LR reaction intermediates were also identified by UPLC-MS/MS to explore the possible degradation pathways of MC-LR. Details of the assay procedure are shown in Text S5.

2.4.5. Identification of ROS

ROS quenching and electron paramagnetic resonance (EPR) tests were performed to offer mechanistic insights into the reactions. ROS trapping experiments were conducted using TBA and IPA as quenching agents for $^{\bullet}OH$, MeOH for $^{\bullet}OH$ and $SO_4^{\bullet-}$, FFA for $^1O_2$, and BQ for $^{\bullet}O_2^-$, respectively. On the other hand, EPR (EMXplus, Bruker, Germany) technique was used to further in situ identify the produced ROS with DMPO and TEMP as trapping reagents. The details of the EPR tests are available in Text S6.

2.5. DFT calculation

All mode structures were employed on the DMol^3 software package. The generalized gradient approximation (GGA) with the Perdew-Burke-Ernzerhof (PBE) exchange-correlation functional to describe electron exchange interaction was selected. For La and Cu elements, the core electrons were replaced by the density functional semicore pseudopotential (DSPP), whereas H, S and O were treated as in the all-electron case. The double numerical plus polarization (DNP) basis set was implemented. During the coordinates relaxation, the total energy was converged to be less than 1.0×10^{-5} hartree, while the forces imposed on each atoms and the displacement convergence were converged to be less than 0.02 hartree $Å^{-1}$ and 0.05 Å, respectively. The vacuum region was set to 15 Å to separate the slabs in the direction perpendicular to the surface. The (020) crystal plane in La_2CuO_4 was used for the construction of the composite material model in this study.

3. Results and discussion

3.1. Characterization of La_2CuO_4 perovskite

XRD patterns of the synthesized La_2CuO_4 perovskite are shown in Fig. 1(A). Clearly, the lattice of the synthesized catalyst well corresponded to the typical orthorhombic La_2CuO_4 (JCPDS No. 80–0579). The diffraction peaks at 24.42°, 27.15°, 31.19°, 33.39°, 41.82°, 43.55°, 47.96°, 58.34°, 65.06° and 85.18° in the catalyst patterns could be attributed to (111), (004), (113), (020), (115), (024), (220), (133), (226) and (335) crystal planes of the orthorhombic La_2CuO_4, respectively. Moreover, the crystalline size was 39.02 nm, and any additional impurity peaks were not observed in the patterns, suggesting a high purity of the La_2CuO_4 perovskite. The N_2 adsorption-desorption isotherms and corresponding pore size distributions of La_2CuO_4 perovskite are presented in Fig. 1(B). The calculated BET specific surface area was 3.24 m^2/g, while the pore volume was 0.016 cm^3/g. Moreover, the perovskite displayed a typical IV isotherm pattern with a narrow type of H3 hysteresis loop and a narrow pore size distribution within 20 nm base on the IUPAC classification, suggesting the presence of mesoporous structure in La_2CuO_4 perovskite [28]. The surface functional groups of La_2CuO_4 perovskite were investigated using FTIR, as shown in Fig. S1. The broad band at near 1450 cm^{-1} was associated with the bending vibration of H-O-H due to the water molecules adsorbed on La_2CuO_4 surface. Meanwhile, the sharp band at 682 cm^{-1} could be attributed to the La-O stretching vibration of the orthorhombic La_2CuO_4 [29]. The surface morphology and microstructures of La_2CuO_4 perovskite are presented in Fig. 1(C). The corresponding elemental distribution was explored using energy dispersive spectroscopy (EDS) and SEM elemental mapping analysis (Fig. 1(D)). Specifically, La_2CuO_4 was composed of regular nanorods with an average length of 150–300 nm. And La, Cu and O elements existed on the perovskite surface with an atomic ratio approximately at 1.75:1:3.68, indicating the catalyst is probably oxygen-deficient $La_2CuO_{4-\delta}$. Besides, the SEM elemental mapping revealed that all the component elements were uniformly distributed on the La_2CuO_4 surface.

Chemical composition and metallic states of La_2CuO_4 perovskite

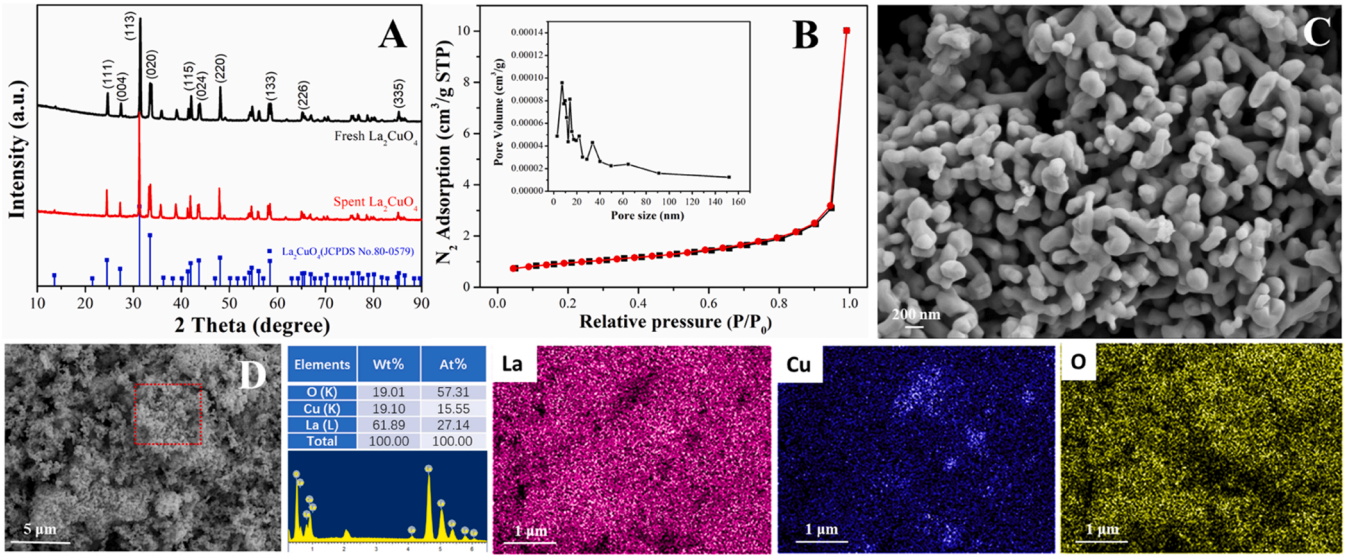

Fig. 1. The XRD patterns (A), N_2 adsorption-desorption isotherms and the correspondent pore size distribution (B), SEM image (C), EDS spectra and mapping (D) of La_2CuO_4 perovskite.

were analyzed by XPS, as shown in Fig. 2. A full spectra revealed the coexistence of La, Cu, O, and C in La_2CuO_4 (Fig. 2(A)). Specifically, La was present in the form of La^{3+} since the typical peaks of La $3d_{3/2}$ and La $3d_{5/2}$ could be assigned to La(III) in the catalyst in Fig. 2(B) [24]. In the Cu 2p spectrum (Fig. 2(C)), two main characteristic peaks of Cu $2p_{1/2}$ and Cu $2p_{3/2}$ were located at 953.2 eV and 932.5 eV, along with shake-up satellite peaks centered at 961.7 eV and 942.2 eV, respectively [30]. The sharp peaks corresponding to Cu $2p_{3/2}$ could be deconvoluted into two peaks, from which the peaks at 933.8 eV and 932.5 eV could be attributed to the oxidation (i.e., Cu^{2+}) and reduction (i.e., Cu^{+}) states of the copper species, respectively [31]. The shake-up peak of Cu $2p_{3/2}$ nearly at 942.2 eV could be assigned to the Cu^{2+} satellite. The aforementioned findings demonstrated that the redox pairs of Cu^{2+}/Cu^{+} was involved in La_2CuO_4 with the relative ratio of 45.4% and 54.6%,

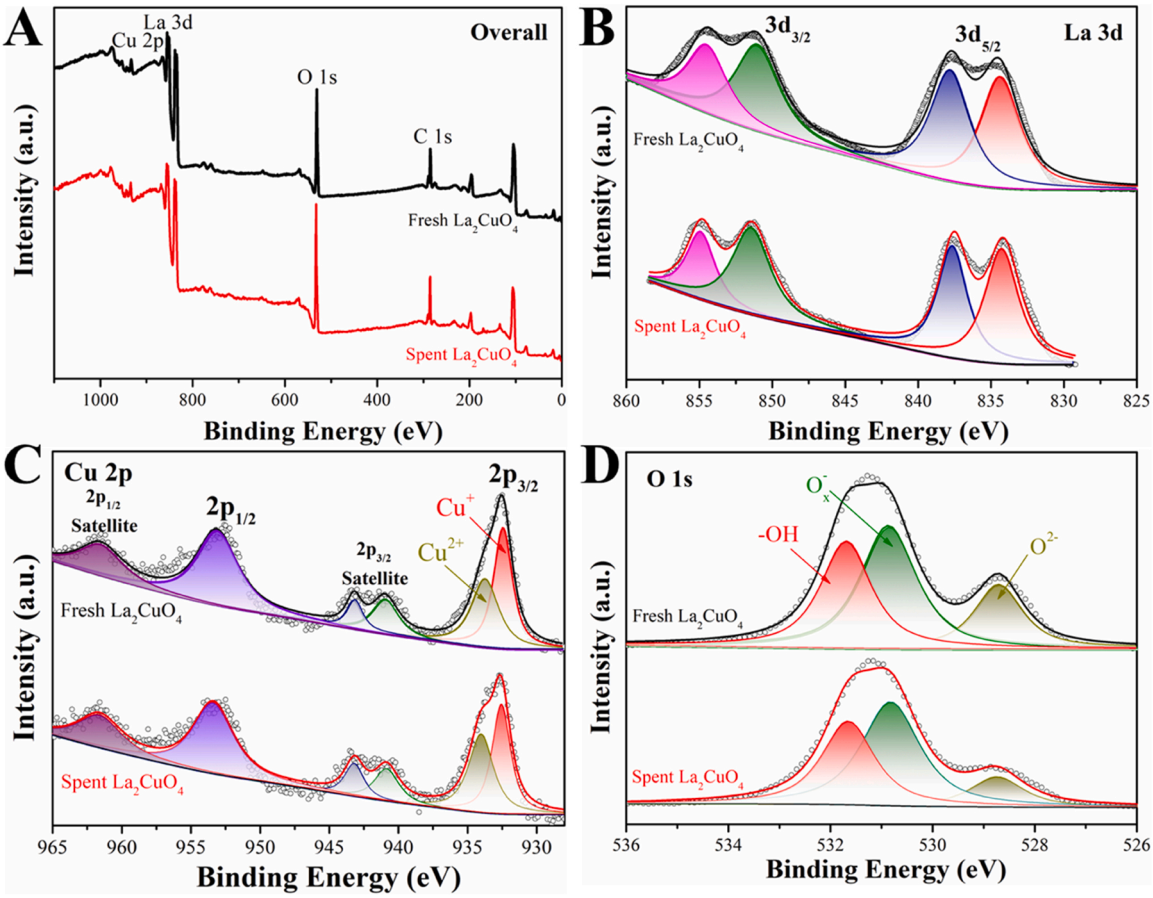

Fig. 2. The XPS spectra of survey scan (A), La 3d (B), Cu 2p (C), and O 1 s (D) in fresh and spent La_2CuO_4 perovskites.

separately. Moreover, the high-resolution XPS spectrum of O 1 s was analyzed to investigate the composition of the oxygen species in La_2CuO_4 in Fig. 2(D). The spectrum could be deconvoluted into three main peaks at 531.7, 530.9 and 528.7 eV, corresponding to adsorbed molecular water (-OH), surface adsorbed oxygen (O_x^-: O_2^{2-}, O^-) and lattice oxygen (O^{2-}), respectively [32]. Their respective proportions were 35.2%, 45.0% and 19.8%. And the adsorbed oxygen with the relatively high content was associated with the generation of oxygen vacancies. Besides, EPR technique was utilized to in situ identify the presence and concentration of oxygen vacancies in La_2CuO_4 perovskite. As shown in Fig. S2, the noticeable signal of electrons trap with g = 2.0 was ascribed to the surface oxygen vacancies. And the existence of Cu^+ species was mainly due to the release of lattice oxygen and the formation of oxygen vacancies in La_2CuO_4 perovskite in the combustion synthesis procedure [33,34], which is consistent with the EDS characterization and XPS results. All the aforementioned results suggested that reductive copper and oxygen vacancies co-existed in the La_2CuO_4 perovskite, creating favorable conditions for the PMS activation.

3.2. Catalytic removal of *M. aeruginosa*

3.2.1. Effect of La_2CuO_4 and PMS dosages

Catalytic treatment of *M. aeruginosa* were evaluated at different mass ratios of La_2CuO_4 to PMS (i.e., La_2CuO_4:PMS), as shown in Fig. 3(A). And the corresponding photographs of *M. aeruginosa* suspensions were exhibited in Fig. S3. The control experiments indicated that 300 mg/L La_2CuO_4 perovskite alone removed approximately 10% of algae cells within 20 min, exhibiting a poor adsorption removal. Similarly, nearly 19% of algal cells were abated by 0.24 mM PMS alone due to PMS-driven chemical oxidation [35]. Notably, the removal efficiency of algal cells significantly improved from 12% to 97% by increasing La_2CuO_4:PMS from 1:1 to 4:1 but declined to 78% in the condition of 5:1. The aforementioned results disclosed that a higher dosage of La_2CuO_4 perovskite might produce more reactive oxygen species (ROS) for PMS activation to promote the catalytic activity and then the algal cells were finally removed. However, superfluous perovskite might flocculate and precipitate, reducing the contact area between the catalyst and *M. aeruginosa* and decreasing the algae removal efficiency, which was consistent with the results reported in the literatures [17,36]. And excessive ROS might also be unfavorably consumed by self-quenching reactions (Eqs. (1)–(3)) [37,38], reducing the catalytic activity. Accordingly, a complete removal of algae cells was achieved within 20 min at 300 mg/L La_2CuO_4 and 0.24 mM PMS with an obvious and rapid settlement of algal cells (Fig. S3). The pseudo 1st-order reaction rate constant of 0.1304 min^{-1} was 25.1 and 15.5 times greater than those of La_2CuO_4 alone (k = 0.0052 min^{-1}) and PMS alone (k = 0.0084 min^{-1}), respectively (Fig. S4).

$$SO_4^{\bullet-} + {}^{\bullet}OH \rightarrow HSO_5^- \quad (1)$$

$$SO_4^{\bullet-} + SO_4^{\bullet-} \rightarrow S_2O_8^{2-} \quad (2)$$

$$SO_4^{\bullet-} + HSO_5^- \rightarrow SO_5^{\bullet-} + SO_4^{2-} + H^+ \quad (3)$$

The removal efficiencies of *M. aeruginosa* using chlorophyll-a as the measurement index in PMS alone, La_2CuO_4 alone, and La_2CuO_4/PMS systems under the optimal dosages are illustrated in Fig. 3(B). It can be seen that only 12% and 11% chlorophyll-a were removed by PMS alone (k = 0.0041 min^{-1}) and La_2CuO_4 alone (k = 0.0064 min^{-1}), respectively. However, a complete removal of chlorophyll-a was achieved within 20 min in the La_2CuO_4/PMS system (k = 0.1814 min^{-1}) (Fig. S5). The findings are consistent with the results for algal cells removal. All the results indicated that PMS in the presence of La_2CuO_4 perovskite could effectively and rapidly remove *M. aeruginosa*, but the removal by the PMS or La_2CuO_4 only was very limited (< 20%), suggesting that the efficient removal of algal cells could be attributed to degradation rather than adsorption in the La_2CuO_4/PMS system. Subsequently, it was compared with other persulfate catalytic systems reported before for removal of *M. aeruginosa*, as shown in Table 1. It can be seen that La_2CuO_4/PMS system exhibited outstanding catalytic activity compared with other homogeneous or heterogeneous catalysts under the optimal dosage, suggesting that the La_2CuO_4 perovskite activated PMS system provides a promising alternative for the control of cyanobacterial blooms with high-efficiency and cost-effectiveness.

3.2.2. PMS utilization efficiency

Meanwhile, the kinetics of PMS decomposition was measured as shown in Fig. 4(A). Only 7% PMS decayed within 20 min in the PMS alone system. In contrast, La_2CuO_4 perovskite effectively activated PMS to result in 71% of PMS decomposition within 20 min, in consistent with the high algae removal efficiency. Correspondingly, the reaction rate constant of PMS decomposition was 0.0721 min^{-1} in the presence of La_2CuO_4/PMS, which was 26.7 times greater than that of PMS alone (Fig. S6). Taking practical applications into consideration, it should be noted that the theoretical value of introducing sulfate into water was 106.5 mg/L, which was below the standard of 250 mg/L in drinking water [39].

3.2.3. Effect of velocity gradient

In addition, to further analyze the algae coagulation process, the effect of velocity gradient on *M. aeruginosa* removal efficiency was studied in Fig. 4(B). It was noteworthy that more and larger algal flocs with a faster settling speed formed under the rapid-slow-stationary reaction process (control) in the La_2CuO_4/PMS system in Fig. S7.

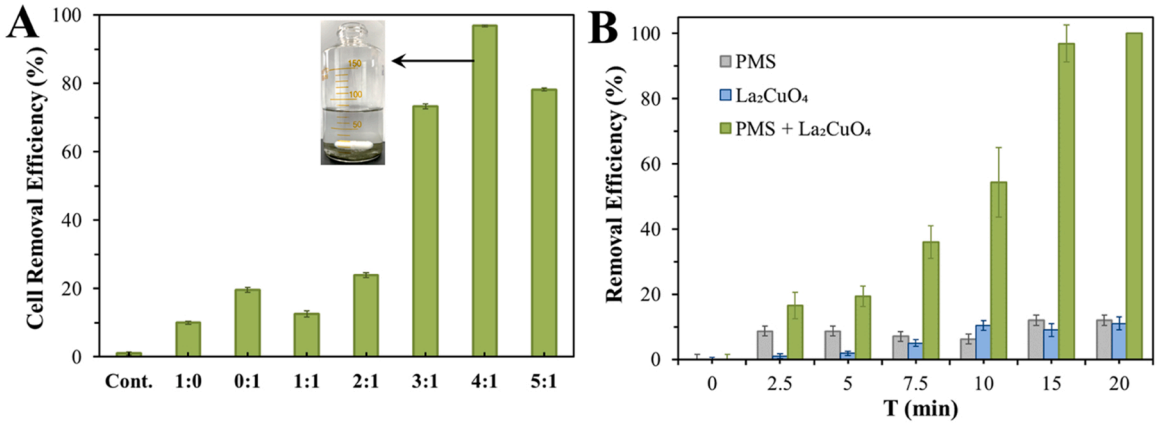

Fig. 3. The removal efficiency of *M. aeruginosa* cells within 20 min by different mass ratio of La_2CuO_4 to PMS (A). The removal efficiency of chlorophyll-a in PMS alone system, La_2CuO_4 alone system, and La_2CuO_4/PMS system (B). Conditions: La_2CuO_4 = 300 mg/L, PMS = 0.24 mM, pH = 7.0, T = 25 °C.

Table 1
Comparison of different catalytic systems for removal of *M. aeruginosa*.

Catalysts	Catalysts dosage	Oxidants dosage	Algae density (cells/mL)	Removal rates	MC-LR removal rates	Main ROS	Ref.
-	-	0.2 mM PMS	(0.93–1.02) × 10^7	100% (48 h)	15 μg/L (3 h)	PMS, $SO_4^{\bullet-}$,$^{\bullet}OH$,$^1O_2$	[35]
$FeSO_4$	13.7 mg/L	50 μM PMS	2 × 10^6	92.3% (20 min)	68.3%	$SO_4^{\bullet-}$,$^{\bullet}OH$	[70]
$FeSO_4$	10 mg/L	84 μM PDS	2.8 × 10^7	95.38% (60 min)	-	$SO_4^{\bullet-}$,$^{\bullet}OH$	[71]
$FeCl_3$	29.2 mg/L	1 mM PMS	(3.48 ± 0.18) × 10^6	97.5% (90 min)	80%	$SO_4^{\bullet-}$,$^{\bullet}OH$	[62]
TP@Fe_3O_4	100 mg/L	0.49 mM PMS	1.74 × 10^7	99% (5 min)	94% (UV 3.5 h/PMS 1.72 mM)	$SO_4^{\bullet-}$,$^{\bullet}OH$,$^1O_2$	[72]
Natural pyrite	1 g/L	1.2 mM PDS	(3.5 ± 0.5) × 10^6	92.8% (360 min)	-	$SO_4^{\bullet-}$,$^{\bullet}OH$,$^{\bullet}O_2^-$,$^1O_2$	[45]
Fe@g-C_3N_4	400 mg/L	0.33 mM PMS	-	93% (30 min)	70% (180 min)	$^1O_2$	[73]
Fe@g-C_3N_4	2 g/L	4 mM PDS	2.5 × 10^6	92% (15 min)	0.6 μg/L (2 h)	$SO_4^{\bullet-}$,$^{\bullet}OH$,$^1O_2$	[74]
La_2CuO_4	300 mg/L	0.24 mM PMS	(2.5 ± 0.5) × 10^6	97% (20 min)	0.35 μg/L (30 min)	$^{\bullet}OH$, $SO_4^{\bullet-}$,$^1O_2$,$^{\bullet}O_2^-$	This study

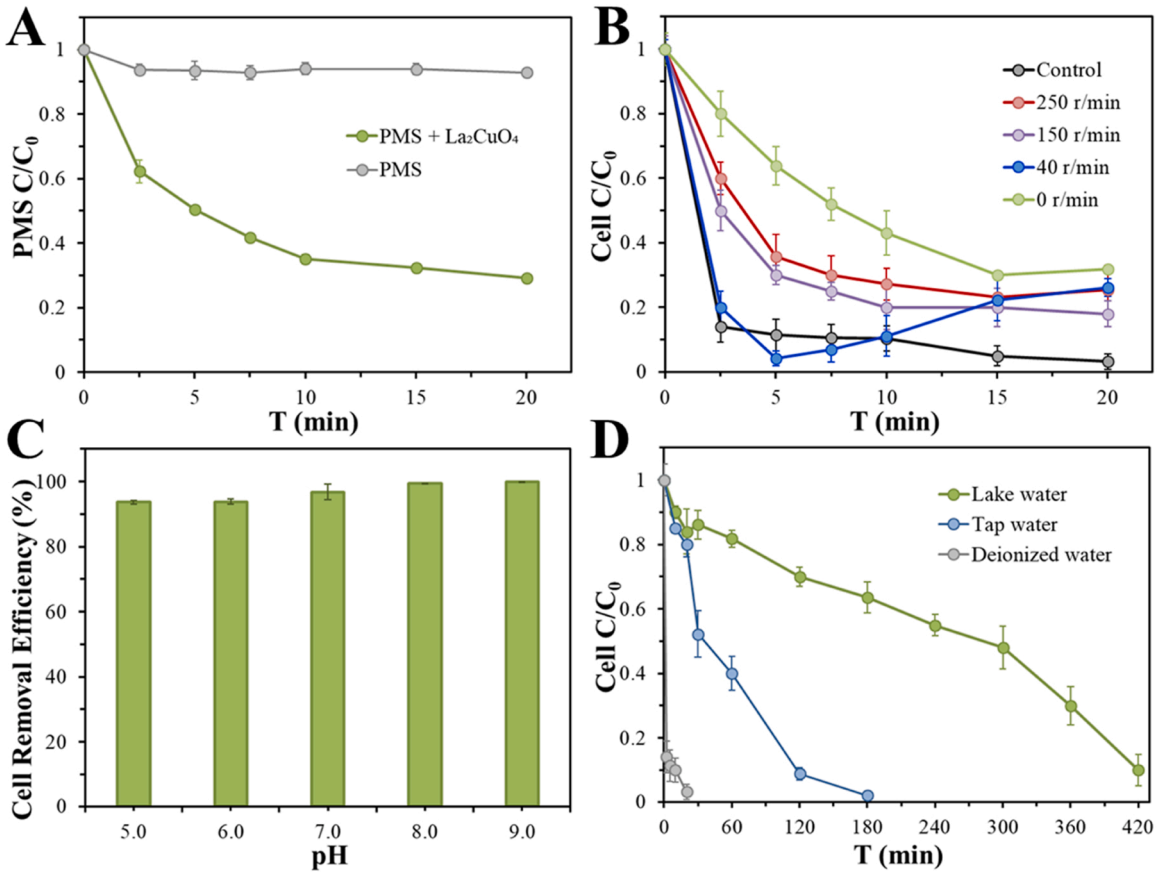

Fig. 4. PMS decomposition efficiency in PMS alone system and La_2CuO_4/PMS system (A). Effects of stirring speed (B), solution pH (C), and water matrix (D) on *M. aeruginosa* removal efficiency. Conditions: La_2CuO_4 = 300 mg/L, PMS = 0.24 mM, pH = 7.0, T = 25 °C.

However, lower algal removal efficiency with the formation of fewer and smaller algal flocs was observed under continuous rapid stirring (250 r/min), medium stirring (150 r/min), slow stirring (40 r/min) or standing (0 r/min), in comparison with the control treatment. Particularly, algal flocs could not be formed well under continuous rapid mixing and stationary condition. For the group with a slow stirring speed, the algal cells were completely removed within 5 min but then regrew with an ultimate removal efficiency of 70%. All the results suggested that a mixing speed significantly affected the algal removal in the catalyst-PMS system, and coagulation and oxidation processes might take place simultaneously for algae removal. In previous studies, AOPs-based reaction systems served as peroxidation, such as UV/H_2O_2, UV/PS and Fe^{2+}/PMS, enhancing the subsequent coagulation-sedimentation of algal cells [15,16,40]. In this study, the better algal removal was likely ascribed to the production of sufficient $^{\bullet}OH$ and $SO_4^{\bullet-}$ in the La_2CuO_4/PMS system, thus facilitating the inactivation of algae cells and prompting growth of flocs.

3.2.4. *Effect of water matrix*

To further evaluate the feasibility of the La_2CuO_4/PMS system in the

treatment of realistic *M. aeruginosa*-laden water, the effect of solution pH and ionic strength on algae removal was evaluated. As seen, the variation of the initial pH (5.0–9.0) exhibited a limited effect in the inhibition of the *M. aeruginosa* removal (Fig. 4(C)). The final pH remained approximately at 6.0 after the catalytic reaction (Fig. S8). Specifically, $\geq$ 95% removal efficiency could be ensured at the acidic and alkaline conditions, suggesting that the performance of the La_2CuO_4/PMS system is independent of pH. In addition, the ionic strength (IS) was adjusted by 0–100 mM $NaNO_3$, and insignificant effect of IS was also obtained on *M. aeruginosa* removal (Fig. S9), revealing that the La_2CuO_4/PMS system possessed strong tolerance to IS in water and an inner-sphere interaction might exist between PMS and active sites of La_2CuO_4 catalyst. Moreover, the treatment was also validated in different water matrixes (Fig. 4(D)), and the main characteristics of practical water samples are provided in Table S2. La_2CuO_4 perovskite could achieve effective algae removal efficiency of $\geq$ 95% in natural Xixi Wetland lake water, tap water and deionized waters within 420 min, 180 min and 20 min, respectively. Of note, the reaction rates were slowed in the natural water bodies likely due to the scavenging of natural organic matter (NOM) (Fig. S10) [26]. However, an effective removal of algae could be achieved. Overall, the La_2CuO_4 activated PMS system adapted to the pH and ionic strength change, while its performance is validated in different water matrixes.

3.2.5. Algal cellular morphology

Extracellular morphological changes of *M. aeruginosa* cells were investigated using SEM to explore the influence of ROS produced in the La_2CuO_4/PMS system on cellular morphology (Fig. 5). *M. aeruginosa* cells possessed regular spherical shape with intact and smooth surface in the control group, accompanied by some natural metabolites as shown in Fig. 5(A) and (B). By contrast, PMS alone caused a rough and deformed cell surface as well as more secretions due to the moderate oxidative activity of PMS in Fig. 5(C) and (D). Meanwhile, La_2CuO_4 perovskite alone accelerated the coagulation process by binding to algal cells without damaging the cell integrity, as indicated in Fig. 5(E) and (F). However, the *M. aeruginosa* cells treated in the La_2CuO_4/PMS system showed extremely irregular and shrunk surface with severe membrane destruction and aggregated nanomaterials in Fig. 5(G) and (H). These findings revealed that La_2CuO_4 catalyst could effectively attach to the surface of algal cells and then the produced reactive species effectively damaged the cells membrane, resulting in the algal cells inactivation and the destruction of extracellular and intracellular substances.

3.2.6. Integrity of algal cells membrane

Taking into account the disruption of the cells membrane and the potential release of intracellular substances, it is necessary to evaluate variation of dissolved organic carbon (DOC) in water, which is a key indicator of water quality in *M. aeruginosa*-laden water treatment. As displayed in Fig. 6(A), even though the algae growth could be inhibited in the PMS alone system [35], DOC in algae suspensions continued to grow. At 120 h, DOC significantly increased from initial condition of 9.5 mg/L to 25.2 mg/L in the PMS alone group, indicating that the algal cells membrane was oxidized and damaged, but the released organic matter could not be effectively removed by PMS alone. On the other hand, DOC of the algae suspension in the La_2CuO_4/PMS system rapidly declined and then gradually increased to 14 mg/L due to the disruption of cells membrane and the apoptosis of cells. Of note, DOC was much lower than that in the PMS alone system, implying that the released organic matter was then effectively oxidized by ROS produced from the La_2CuO_4/PMS system, which can mitigate the impact of the released organics in subsequent water treatment. The variations of K^+, Ca^{2+} and Mg^{2+} release in the La_2CuO_4/PMS system are illustrated in Fig. 6(B). The release of these cations can indirectly indicate the degree of cell membrane integrity, because they are the main ingredients of biosynthesize cytoplasmic membrane [40]. As seen, their concentrations significantly grew as time, before peaking at 25, 3 and 1 mg/L, respectively, which is similar to the findings reported elsewhere [15,41]. The large amount of released K^+, Ca^{2+} and Mg^{2+} ions distinctly indicated that the algal cells membrane integrity was greatly damaged by the produced ROS. Moreover, it was noteworthy that the final Cu^{2+} concentration after the *M. aeruginosa*-laden water treatment reached a steady state of 0.65 mg/L, which is well below the drinking water regulations in the U. S. (1.3 mg/L) and EU (2 mg/L) [42]. However, the equivalent Cu^{2+} activated PMS system only resulted in a limited *M. aeruginosa* removal of 48% (Fig. S11), suggesting that the outstanding algae removal efficiency can be attributed to the heterogeneous catalysis of La_2CuO_4 perovskite. In brief, all the aforementioned results demonstrated that the La_2CuO_4/PMS system was an efficient process to remove *M. aeruginosa* without a severe increase of DOC and metal concentrations in water, ensuring the safety of its practical application.

3.3. Reaction mechanisms

3.3.1. Change of algal organic matter

In the process of catalytic inactivation of *M. aeruginosa*, toxic algal organic matter (AOM) was commonly released to water, which may be the potential precursors of disinfection by-products (DBPs) in the subsequent chlorination process [17]. Hence, three-dimensional fluorescence excitation emission matrixes (3D-EEMs) spectroscopy was employed to explore the influence of La_2CuO_4/PMS system on the variations of AOM. As shown in Fig. 7, four fluorescence peaks are identified, which are located at $\lambda_{ex}/\lambda_{em}$ = 275/320 nm (peak A), 220/320 nm (peak B), 350/450 nm (peak C), and 275/450 nm (peak D),

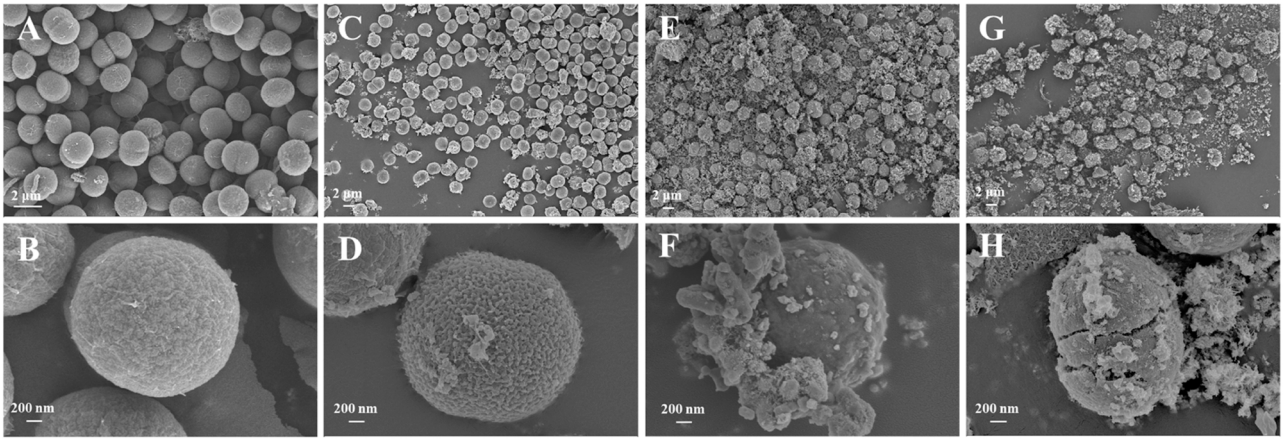

Fig. 5. The surface morphology of *M. aeruginosa* cells observed via SEM in different reaction systems: control (A and B), PMS alone system (C and D), La_2CuO_4 alone system (E and F), and La_2CuO_4/PMS system (G and H).

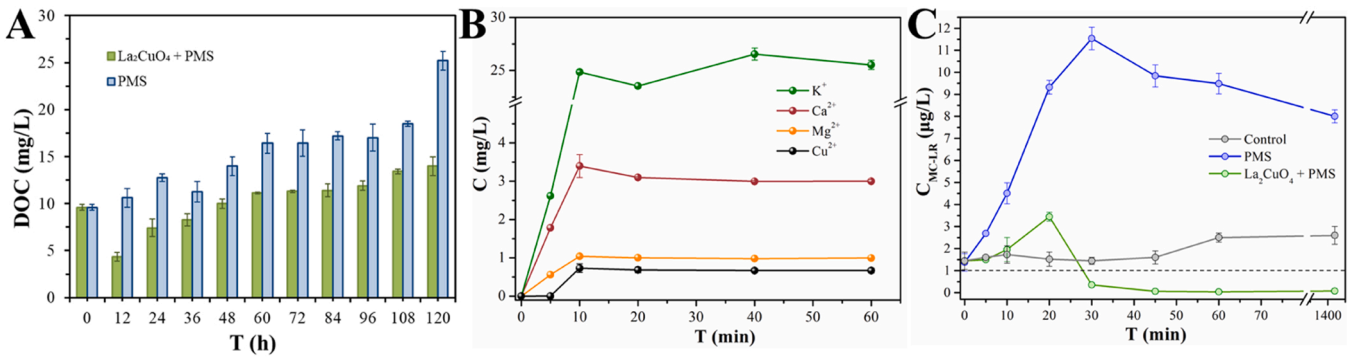

Fig. 6. The DOC variations after algae being cultivated for 5 d in PMS alone system and La_2CuO_4/PMS system (A). Release of residual metal ions (B) and extracellular MC-LR (C) in the La_2CuO_4/PMS system. Conditions: La_2CuO_4 = 300 mg/L, PMS = 0.24 mM, pH = 7.0, T = 25 °C.

corresponding to dissolved microbial metabolites, aromatic protein (tyrosine and tryptophan), humic acid-like and fulvic acid-like substances, respectively [43]. More specifically, dissolved microbial metabolites and aromatic protein can be attributed to the release of normally physiological metabolism. Oxidative decomposition of macromolecular organic matter or normally apoptotic algal cells might be responsible for humic acid-like and fulvic acid-like substances [44]. The high intensities of both peaks A and B for AOM suggested that considerable dissolved microbial metabolites and aromatic protein were involved in both extracellular organic matter (EOM) and intracellular organic matter (IOM) during the algal growth process (0 min). It was worth mentioning that the intensities of the peaks A and B were both distinctly alleviated in EOM and IOM with prolonged reaction time after the La_2CuO_4/PMS treatment, indicating that accompanied by the rupture of the algal cells membrane, dissolved microbial metabolites and aromatic protein were released extracellularly, which were then preferentially oxidized by the ROS produced in the La_2CuO_4/PMS system due to their strong hydrophilicity and poor aggregation ability [45]. In addition, the intensities of both peaks C and D in EOM were dramatically increased at 5 min in the La_2CuO_4/PMS system, but the counterparts in IOM were sharply mitigated, likely because of the rupture of the algae cells. It should be noted that humic acid-like and fulvic acid-like substances in both EOM and IOM gradually decayed until vanishing at 60 min. On the contrary, the strengthened intensities of both peaks C and D in EOM without a noticeable decrease over reaction time were observed in the PMS alone system (Fig. S12). The intensities were many orders of magnitude higher than those of the La_2CuO_4/PMS system, in consistence with the continuously increased DOC. Meanwhile, the intensities of both peaks A and B in IOM were not significantly reduced in the PMS alone system due to the limited damage to algal cells by the PMS oxidation (Fig. S13). Therefore, the aforementioned results revealed that a La_2CuO_4/PMS system could not only promote the catalytic inactivation of *M. aeruginosa*, but also further degrade the released AOM without a concern over the production of secondary contaminants, as evidenced by the evolution of DOC, K^+, Ca^{2+} and Mg^{2+} concentrations.

3.3.2. Identification of reactive oxygen species

To explore the contributions of various ROS produced in the La_2CuO_4/PMS system to the catalytic inactivation of *M. aeruginosa*, ROS quenching tests were carried out using methanol (MeOH), isopropanol (IPA), *t*-butanol (TBA), furfuryl alcohol (FFA) and *p*-benzoquinone (BQ) as different ROS scavengers. More specifically, MeOH can promptly react with free $^{\bullet}OH$ and $SO_4^{\bullet-}$ in bulk solution with high reaction rate constants of 9.7×10^8 and 2.5×10^7 M^{-1} s^{-1}, respectively. Nevertheless, IPA can quench both of surface-bound and free $^{\bullet}OH$ and $SO_4^{\bullet-}$ due to the lower dielectric constants and higher affinity ($k_{IPA, \bullet OH} = 1.9 \times 10^9$ M^{-1} s^{-1}, $k_{IPA, SO4\bullet-} = 8.2 \times 10^7$ M^{-1} s^{-1}). TBA was used as a specific scavenger for $^{\bullet}OH$ ($k_{TBA, \bullet OH} = 3.8–7.6 \times 10^8$ M^{-1} s^{-1}), rather than $SO_4^{\bullet-}$ ($k_{TBA, SO4\bullet-} = 4.0–9.5 \times 10^5$ M^{-1} s^{-1}). Besides, FFA and BQ were commonly used as probe compounds for $^1O_2$ ($k_{FFA, 1O2} = 1.2 \times 10^8$ M^{-1} s^{-1}) and $^{\bullet}O_2^-$ ($k_{BQ, \bullet O2-} = 2.9 \times 10^9$ M^{-1} s^{-1}), respectively [32,46–49]. As illustrated in Fig. 8(A), *M. aeruginosa* cells were almost completely removed in 20 min without scavenger (97%). The addition of MeOH did not have a significant inhibition effect on the catalytic performance, whereas the removal efficiencies at 20 min were 10% and 73% with the addition of IPA and TBA, respectively, suggesting that *M. aeruginosa* might be catalytically inactivated by surface-bound $^{\bullet}OH$ and $SO_4^{\bullet-}$ produced in the La_2CuO_4/PMS system. The limited inhibition effects of FFA and BQ indicated that little $^1O_2$ and $^{\bullet}O_2^-$ were produced in the catalysis. Moreover, it should be noted that the presence of a scavenger alone limitedly suppressed the algal growth (Fig. S14), suggesting that the catalytic inactivation of *M. aeruginosa* could be ascribed to the ROS produced in the La_2CuO_4/PMS system rather than the toxicity of scavengers. In the catalytic inactivation process, surface-bound $^{\bullet}OH$ and $SO_4^{\bullet-}$ are plausibly responsible for algae inactivation as the main active species.

Furthermore, the electron paramagnetic resonance (EPR) technique was used to validate the production of in-situ active species from the La_2CuO_4 activated PMS system for algae inactivation. Specifically, 5,5-dimethyl-1-pyrroline (DMPO) was used as a spin trap to identify $^{\bullet}OH$ and $SO_4^{\bullet-}$ by forming spin adducts DMPO-$^{\bullet}OH$ and DMPO-$SO_4^{\bullet-}$, respectively. As displayed in Fig. 8(B), compared with the DMPO itself and the PMS alone system, a typical spectral characteristic quadruple of DMPO-$^{\bullet}OH$ with a robust peak intensity ratio of 1:2:2:1 was observed in the La_2CuO_4/PMS system. A minor signal of DMPO-$SO_4^{\bullet-}$ was also observed, likely because that the short-lived adducts ($t_{1/2}$ = 95 s in water) rapidly converted to DMPO-$^{\bullet}OH$ through the nucleophilic substitution reactions [23,50]. Meanwhile, distinct DMPO-$^{\bullet}O_2^-$ signal appeared using DMPO as the spin trapping agent in methanol solution in the La_2CuO_4/PMS system in Fig. 8(C) [51,52], and the typical triplet (1:1:1) spectrum appeared with 2,2,6,6-tetramethyl-4-piperidinol (TEMP) as the capture agent in Fig. 8(D), suggesting that $^{\bullet}O_2^-$ and $^1O_2$ were generated during the PMS activation and the generated $^1O_2$ may derived from the disproportionation of $^{\bullet}O_2^-$. The findings were well consistent with those in the aforementioned classical quenching tests, demonstrating that $^{\bullet}OH$, $SO_4^{\bullet-}$, $^1O_2$ and $^{\bullet}O_2^-$ were the oxidizing species all responsible for the *M. aeruginosa* inactivation and subsequent AOM removal. Among them, surface-bound $^{\bullet}OH$ and $SO_4^{\bullet-}$ played an essential role.

3.3.3. Possible catalytic mechanisms

Single component control experiments of La_2O_3 and CuO for algae inactivation were also carried out to further explore the key active ingredients in the La_2CuO_4 perovskite. Surprisingly, only 40% of the algae were removed within 20 min in an equivalent CuO/PMS system in Fig. S15(A), although copper oxide has proven to be an effective catalyst in activating PMS [53]. However, a complete inactivation of

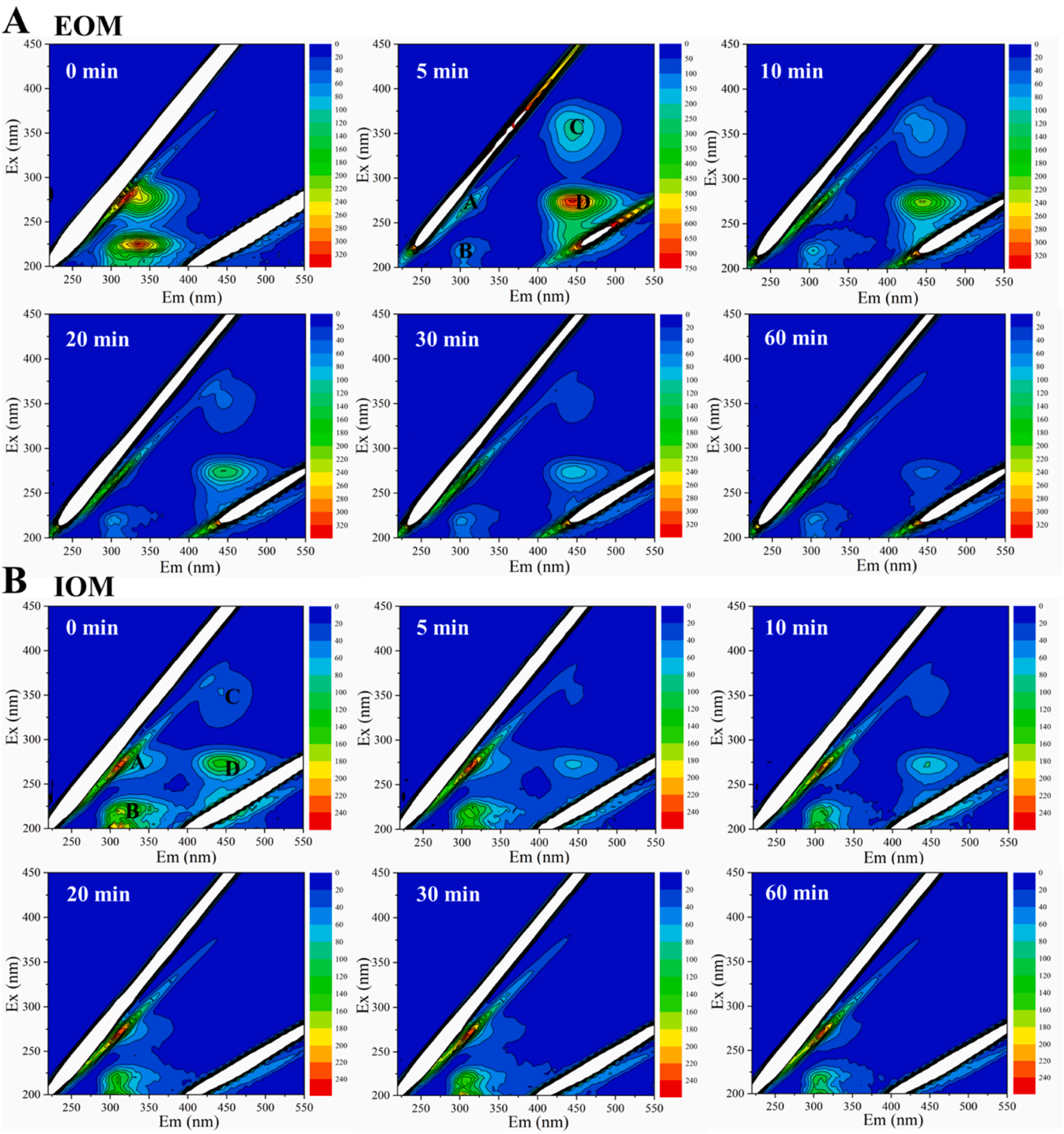

Fig. 7. The fluorescence EEMs spectra of EOM and IOM: 0 min, 5 min, 10 min, 20 min, 30 min and 60 min in the La_2CuO_4/PMS system.

M. aeruginosa was attained within 20 min in the equivalent La_2O_3/PMS system or the physical mixing of La_2O_3 and CuO activated PMS system, in agreement with the results of the La_2CuO_4/PMS system, though La_2O_3 cannot effectively activate PMS due to the absence of variable valence elements. Besides, it was worth mentioning that the catalyst alone, such as La_2CuO_4, La_2O_3, CuO, and physical mixing of La_2O_3 and CuO, poorly inactivated algae, as shown in Fig. S15(B). Thereby, it was speculated that the La portion in La_2CuO_4 perovskite might play a crucial role for *M. aeruginosa* inactivation in the PMS catalytic process.

Zeta potential was measured, while ROS identification experiments of single oxide catalytic systems were conducted to understand the underlying information. As displayed in Fig. S16(A), the pH_{PZC} value of CuO is approximately 7.0, while La_2O_3 and La_2CuO_4 are positively charged at pH 7.0, indicating that the excellent *M. aeruginosa* inactivation performance might be attributed to the surface positively charge of catalysts through electrostatic attraction with algae cells. Besides, the absolute value of zeta potential of algae suspension discrepantly decreased in the catalytic systems with the following order: CuO/PMS $<$ La_2O_3/PMS $<$ La_2CuO_4/PMS in Fig. S16(B). Zeta potential of *M. aeruginosa* suspension significantly ranged from −44 to −10 and −15 mV in the La_2CuO_4/PMS system and La_2O_3/PMS system, respectively, suggesting that the reduction in the absolute value of zeta

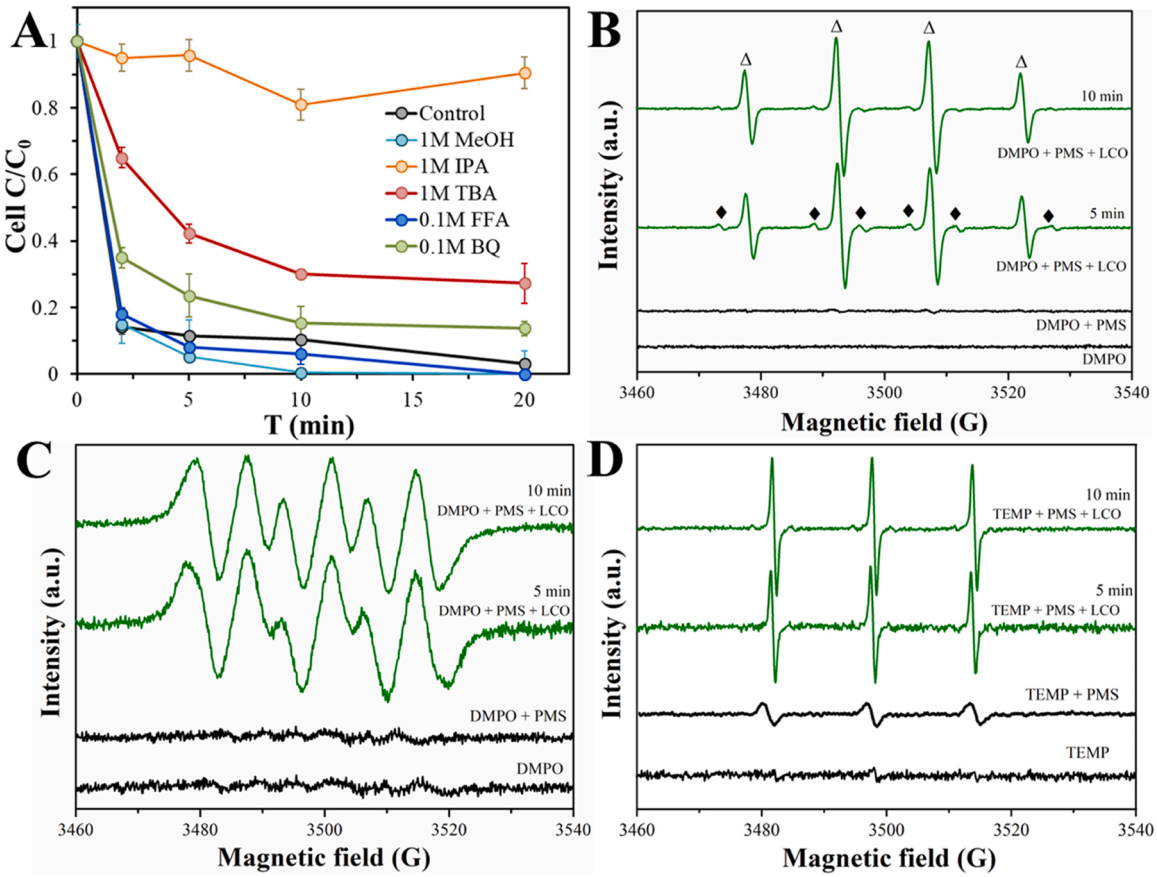

Fig. 8. The removal efficiency of *M. aeruginosa* cells in the La_2CuO_4/PMS system under the addition of various scavengers (A). EPR spectra with DMPO as a trapping agent in ultrapure water for the detection of $^{\bullet}OH$ and $SO_4^{\bullet-}$ (B), in methanol for the detection of $^{\bullet}O_2$ (C), and with TEMP as a trapping agent for the detection of $^1O_2$ (D). Conditions: La_2CuO_4 = 300 mg/L, PMS = 0.24 mM, [DMPO] = 0.02 mol/L, [TEMP] = 0.02 mol/L, pH = 7.0, T = 25 °C. △: DMPO-$^{\bullet}OH$; ◆: DMPO-$SO_4^{\bullet-}$.

potential was a crucial factor for the enhanced *M. aeruginosa* removal. It should be noted that the presence of various catalysts alone did not significantly change the surface potential of algae in Fig. S16(C). The findings indicated that the existence of lanthanum portion rather than copper portion in La_2CuO_4 perovskite could result in the reduction in the absolute value of zeta potential and the improvement of algae coagulation through electrostatic attraction in the PMS catalytic process. On the other hand, as expected, considerable $^{\bullet}OH$ was produced in the CuO/PMS system, but not from a La_2O_3/PMS system (Fig. S17). The cyclic voltammetry (CV) curves in Fig. S18 further revealed that La_2CuO_4 and CuO had higher current density and greater reductive capability than La_2O_3, indicating that copper portion in La_2CuO_4 perovskite could enhance the electron transfer process between perovskite surface and PMS. Therefore, all the aforementioned results demonstrated that the

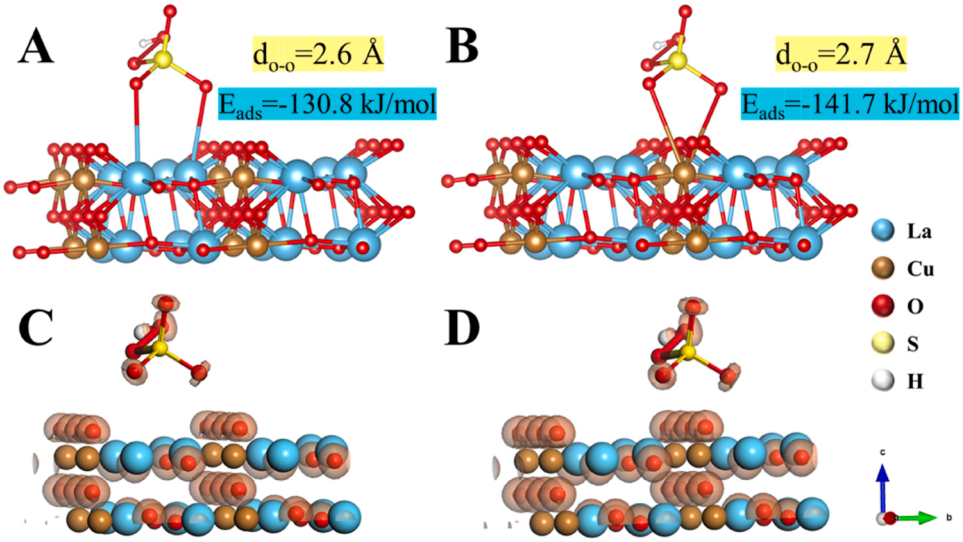

Fig. 9. The adsorption energy (A and B) and charge difference distribution (C and D) of La_2CuO_4/PMS with two different structures.

synergistic effect of La and Cu was responsible for the excellent catalytic activity of La_2CuO_4 perovskite, where the La portion in La_2CuO_4 perovskite could shorten the physical distance between the catalyst and algal cells and benefit the destabilization of algae cells by reducing the absolute value of zeta potential of *M. aeruginosa* suspension through electrostatic attraction. Meanwhile, the variable Cu portion in La_2CuO_4 perovskite facilitated the electron transfer between the catalyst and PMS to generate more active ROS and improved the utilization efficiency of ROS in the microenvironment on the La_2CuO_4 surface.

Theoretical calculation was utilized to reveal the underlying mechanism of enhanced PMS catalytic activation by La_2CuO_4. As shown in Fig. 9, the simulation results indicated that there were two adsorption sites (i.e., La site and Cu site) of PMS on the La_2CuO_4 surface. Compared to the length of the peroxyl bond (d_{o-o}) of PMS on La site of La_2CuO_4 (2.6 Å), the longer d_{o-o} of 2.7 Å was obtained on Cu site of La_2CuO_4, suggesting that Cu active site was more likely to facilitate the cleavage of the O–O bond in PMS (2.3 Å). Meanwhile, the adsorption energy of PMS on Cu site of La_2CuO_4 (141.7 kJ/mol) was much higher than that of PMS on La site of La_2CuO_4 (130.8 kJ/mol), indicating that the electronic structure of Cu would effectively promote PMS adsorption by transferring electron to generate more ROS. In addition, the charge difference distribution (CDD) of La_2CuO_4 after PMS adsorption was also explored in Fig. 9 (C) and (D), and electron transfer from La_2CuO_4 to PMS could be confirmed. Thus, the DFT calculations disclosed that PMS could greatly adsorbed on Cu site of La_2CuO_4 surface by transferring electron to generate ROS, which was consistent with the aforementioned results.

XPS spectra of fresh and spent La_2CuO_4 perovskites were further analyzed to investigate the change in oxidation states of surface elements after the catalytic reaction. As illustrated in Fig. 2(B), there was no significant change of La^{3+} valence in the La 3d spectrum, suggesting that La^{3+} was not involved in the catalytic reaction for PMS activation, which is consistent with the results in Fig. S17. For the Cu 2p spectrum of spent La_2CuO_4 in Fig. 2(C), relative content of Cu^{2+} increased from 45.4% to 49.2% and Cu^{+} decreased from 54.6% to 50.8% after the catalytic reaction, separately, suggesting electron transfer occurred between surface Cu species and PMS to produce ROS, such as surface-bound $^{\bullet}OH$ and $SO_4^{\bullet-}$ (Eqs. (4)–(6)) [23,54], which was well consistent with the aforementioned results. The role of Cu^{3+} has been proved for PMS activation to produce $SO_4^{\bullet-}$ in previous literatures (Eqs. (7)–(9)) [54,55], but Cu^{3+} was not detected in this work. Meanwhile, compared to fresh La_2CuO_4 perovskite for the O 1 s spectrum in Fig. 2(D), the relative contents of adsorbed molecular water (-OH), surface adsorbed oxygen (O_x^-) and lattice oxygen (O^{2-}) obviously changed from 35.2%, 45.0%, 19.8% to 36.4%, 49.5%, 14.1% in spent La_2CuO_4, respectively, indicating that lattice oxygen may participate in PMS activation for the formation of $^1O_2$ or $^{\bullet}O_2^-$. It is well reported that $^{\bullet}O_2^-$ might derive from dissolved oxygen in solution, oxygen vacancies in heterogenous catalysts or hydrolysis of PMS [56–58]. Separate tests were adopted by continuously purging N_2 or O_2 into the solution to evaluate the effect of dissolved oxygen. As shown in Fig. S19, the removal efficiency of *M. aeruginosa* cells was slightly declined, but there was no significant difference between N_2 or O_2 aeration, which could be attributed to the adverse effect of gas disturbance on coagulation settlement of algae cells. Besides, based on the fact that the signal strength of oxygen vacancies did not change significantly in EPR (Fig. S2) and the content of adsorbed oxygen increased distinctly in XPS (Fig. 2(D)) after the catalytic reaction, the formation of $^{\bullet}O_2^-$ through electron donation role of oxygen vacancies could be neglected. Therefore, $^{\bullet}O_2^-$ should originated from hydrolysis of PMS facilitated by La_2CuO_4 catalyst (Eqs. (12)-(13)), and the oxygen species derived from $^{\bullet}O_2^-$ improved the surface adsorbed oxygen content in spent La_2CuO_4 after the catalytic reaction. On the other hand, we proposed the oxygen vacancies dependent $^1O_2$ evolution mechanism over perovskite by decreasing the activation energy of PMS self-decomposition in our previous studies [27], which was inconsistent with the current work that the oxygen vacancies content remained unchanged but the lattice oxygen decreased significantly in La_2CuO_4 perovskite in the process of removing algae. Accordingly, we speculated that the chemisorbed oxygen (O*) transferred from the lattice oxygen could be converted into $^1O_2$ through the catalytic reaction with PMS (Eqs. (14)-(15)) [59,60]. Meanwhile, $^{\bullet}O_2^-$ might also be responsible for the $^1O_2$ production through proton-promoted disproportionation of $^{\bullet}O_2^-$ under acidic conditions during the PMS activation process (Eqs. (16)) [56,61]. In brief, all the ROS produced contributed to the *M. aeruginosa* inactivation and subsequent AOM removal.

$$\equiv Cu^{+} + HSO_5^- \rightarrow \equiv Cu^{2+} + {}^{\bullet}OH + SO_4^{2-} \quad (4)$$

$$\equiv Cu^{+} + HSO_5^- \rightarrow \equiv Cu^{2+} + SO_4^{\bullet-} + OH^- \quad (5)$$

$$\equiv Cu^{2+} + HSO_5^- \rightarrow \equiv Cu^{+} + SO_5^{\bullet-} + H^+ \quad (6)$$

$$\equiv Cu^{2+} + HSO_5^- \rightarrow \equiv Cu^{2+}\text{-}OSO_3^- + OH^- \quad (7)$$

$$\equiv Cu^{2+}\text{-}OSO_3^- \rightarrow \equiv Cu^{3+} + SO_4^{\bullet-} \quad (8)$$

$$\equiv Cu^{3+} + HSO_5^- \rightarrow \equiv Cu^{2+}\text{-}OOSO_3^- + H^+ \quad (9)$$

$$^{\bullet}OH + HSO_5^- \rightarrow SO_5^{\bullet-} + H_2O \quad (10)$$

$$2SO_5^{\bullet-} \rightarrow 2SO_4^{\bullet-} + O_2 \quad (11)$$

$$HSO_5^- + H_2O \rightarrow SO_4^{2-} + HO_2^- + 2H^+ \quad (12)$$

$$HO_2^- + 2HSO_5^- \rightarrow SO_4^{\bullet-} + 2{}^{\bullet}O_2^- + SO_4^{2-} + 3\,H^+ \quad (13)$$

$$O_{Lat} \rightarrow O^* \quad (14)$$

$$O^* + HSO_5^- \rightarrow HSO_4^- + {}^1O_2 \quad (15)$$

$$2{}^{\bullet}O_2^- + 2\,H^+ \leftrightarrow H_2O_2 + {}^1O_2 \quad (16)$$

3.4. Degradation pathways of MC-LR

The cyanotoxins release of MC-LR during the inactivation process of *M. aeruginosa* was measured using the UPLC-MS/MS technique. As shown in Fig. 6(C), very limited MC-LR increase was observed within 24 h in the algae-laden suspension in the control group due to the normal metabolism of *M. aeruginosa*. However, the PMS alone caused severe release in MC-LR (11.5 μg/L), likely owning to the cell damage and subsequent massive release of intracellular MC-LR after the PMS oxidation. PMS could not directly oxidize extracellular MC-LR due to the moderate reactivity of persulfate. As expected, La_2CuO_4/PMS system significantly abated MC-LR, below the recommended value of 1 μg/L as the reference. Specifically, the concentration of extracellular MC-LR slightly increased within 20 min followed by a rapid decrease, because the destruction of algal cells released substantial intracellular MC-LR [62]. In addition, the level of MC-LR in the water was still not elevated after 24 h (< 1 μg/L, Fig. 6(C)) and the La_2CuO_4 perovskite showed weak physical adsorption capacity for MC-LR (Fig. S20), suggesting the released MC-LR was effectively removed by strongly oxidative ROS produced in the La_2CuO_4/PMS system. Consequently, *M. aeruginosa* and MC-LR can be simultaneously removed by the La_2CuO_4 activated PMS system.

MC-LR degradation intermediates in the La_2CuO_4/PMS system were identified to reveal the plausible oxidation pathways. MC-LR ($m/z = 995.6$) and its seventeen degradation intermediates were detected and analyzed under the positive ionization mode using the UPLC-MS/MS technique. The transformation products (TPs) are summarized in Fig. S21 and Table S3. The plausible degradation pathways of MC-LR over the La_2CuO_4/PMS oxidation treatment are proposed in Fig. 10. Specifically, $^{\bullet}OH$ with non-selectivity is required to attack a specific functional group, while $SO_4^{\bullet-}$ with high-selectivity could readily attack multiple electron-rich moieties in MC-LR as a strong electrophilic reagent, such as *Adda*, *Glu*, *Mdha*, *Ala*, *MeAsp* and *Arg* groups via similar pathways of hydrogen abstraction, electron transfer, and addition-

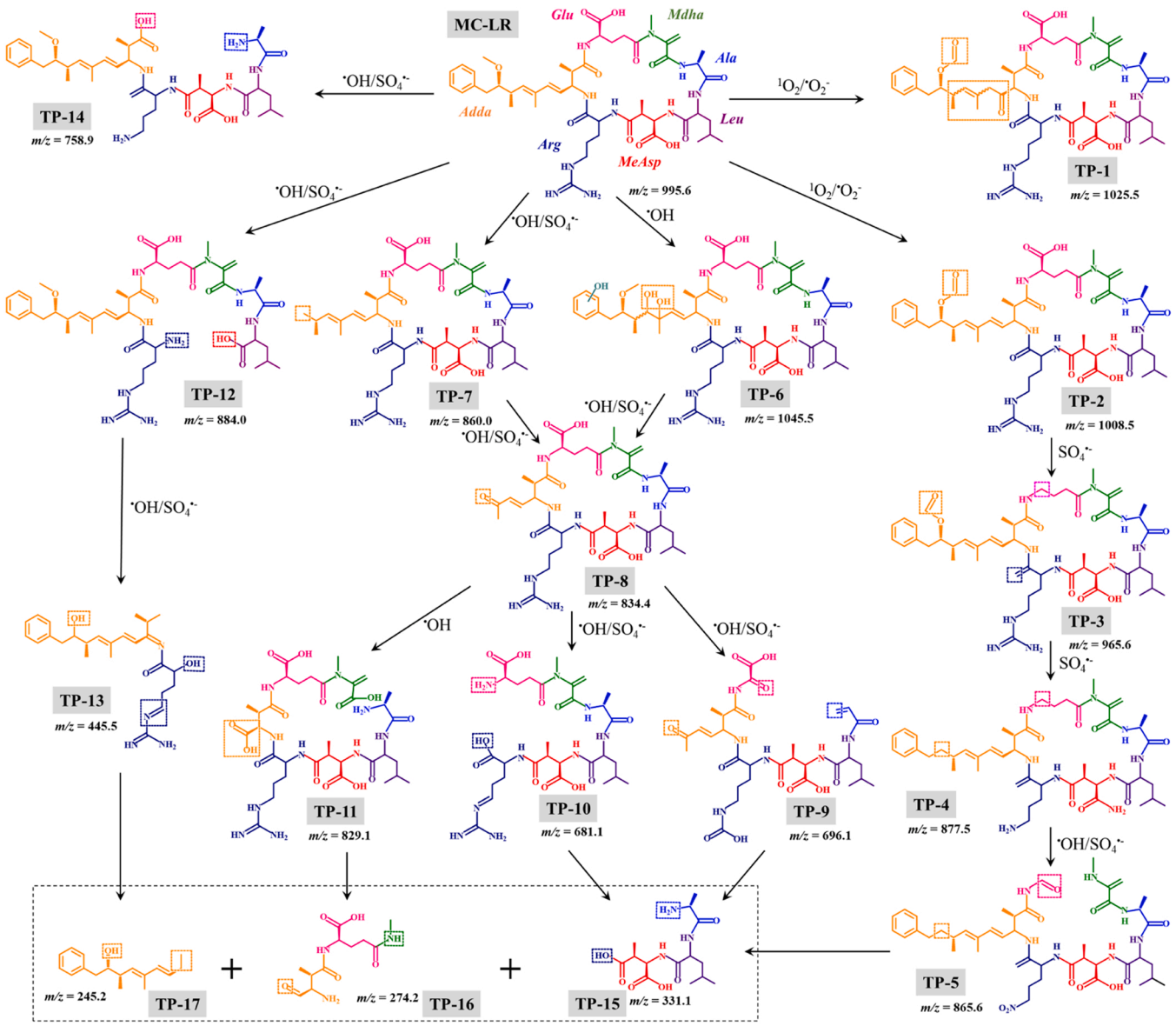

Fig. 10. The plausible degradation pathways of MC-LR during La_2CuO_4/PMS oxidation process.

elimination [63–65]. Besides, $^1O_2$ could attack organics through cycloaddition, and $^{\bullet}O_2^-$ as a nucleophile could attack carbon atoms through nucleophilic substitution. First, the electron-rich unsaturated bonds at the *Adda* moiety validated to serve as the most susceptible sites. TP-1 ($m/z = 1025.5$) and TP-2 ($m/z = 1008.5$) were formed when the methoxy group of MC-LR converted to the aldehyde or carbonyl substitution by $^1O_2$ and $^{\bullet}O_2^-$ with moderate oxidation capacity [66]. Afterward, decarboxylation occurred at *Glu* moiety of TP-2 to form TP-3 ($m/z = 965.6$) and TP-4 ($m/z = 877.5$) by $SO_4^{\bullet-}$ attack, which proved to be unique in $SO_4^{\bullet-}$-AOPs [9]. Finally, TP-5 ($m/z = 865.6$) was produced through the cleavage of C-N bond in *Glu* and *Mdha* groups by $^{\bullet}OH$ and $SO_4^{\bullet-}$ with robust oxidation capacity. Meanwhile, multiple hydroxylation might occur at the diene bond or benzene ring of *Adda* moiety to form TP-6 ($m/z = 1045.5$) due to the $^{\bullet}OH$ attack, followed by the destruction of C-C bonds at *Adda* moiety ($m/z = 860.0$, $m/z = 834.4$) by $^{\bullet}OH$ and $SO_4^{\bullet-}$ oxidation [67]. Further oxidation of *Adda* and *Mdha* moieties in TP-8 led to the production of fragments with $m/z = 829.1$, 696.1 and 681.1 through the cleavage of C-N and C-C bonds by $^{\bullet}OH$ and $SO_4^{\bullet-}$ oxidation, respectively. On the other hand, direct cleavage of MC-LR likely occurred to form TP-14 ($m/z = 758.9$) and TP-12 ($m/z = 884.0$) due to the loss of *Glu*, *Mdha* or *MeAsp* groups, followed by further oxidation of *Adda* moiety ($m/z = 445.5$) by highly oxidizing $^{\bullet}OH$ and $SO_4^{\bullet-}$ [68]. Eventually, these degradation intermediates could be decomposed into smaller molecular substances by the generated oxidizing free radicals ($^{\bullet}OH$, $SO_4^{\bullet-}$), reducing free radicals ($^{\bullet}O_2^-$) as well as non-free radicals ($^1O_2$), such as TP-15 ($m/z = 333.1$), TP-16 ($m/z = 274.2$) and TP-17 ($m/z = 245.2$), suggesting the remarkable mineralization ability in the La_2CuO_4/PMS oxidation of MC-LR. In brief, $^{\bullet}OH$, $SO_4^{\bullet-}$, $^1O_2$ and $^{\bullet}O_2^-$ were the oxidizing species all responsible for MC-LR decomposition, and surface-bound $^{\bullet}OH$ and $SO_4^{\bullet-}$ played a primary role with robust oxidation capacity. These observations are consistent with the results of ROS identification tests, DOC concentration and 3D-EEMs spectroscopy.

3.5. Reusability of La_2CuO_4 perovskite

To examine the stability of La_2CuO_4 perovskite, the structure and morphology of catalyst were characterized before and after the heterogeneous catalytic reaction. The results suggested that the diffraction peaks in XRD patterns (Fig. 1(A)) and microstructures in SEM images (Fig. S22) of spent La_2CuO_4 perovskite did not change significantly, except for the agglomeration of nanorods. Moreover, the reusability of

La_2CuO_4 perovskite was further evaluated via five consecutive cycles. The corresponding algal removal efficiencies were 97%, 76%, 60%, 55%, 53%, respectively, as seen in Fig. S23. The significant decline of catalytic ability may be attributed to several reasons. First, the agglomeration or compaction of catalyst in the process of catalytic reaction might lead to the decrease of active sites in La_2CuO_4 perovskite, which has been confirmed by SEM images (Fig. S22). Secondly, the unavoidable mass loss and metal ion leaching in the process of material regenerating and recycling might reduce the yield of the ROS produced, resulting in a decrease in catalytic activity. Thirdly, the residual algal cell debris or algal organic matters on the surface of catalyst would lead to the reduction of PMS activity. It is worth noting that similar results of reduced catalytic performance after recovery have been reported in many previous literatures [17,24,69]. Briefly, the La_2CuO_4 perovskite is a functionally stable and efficient catalyst for PMS activation to control the cyanobacterial blooms.

4. Conclusions

This study aimed to develop an innovative heterogeneous La_2CuO_4/PMS system for mitigating harmful algal bloom impacts in drinking water supply, with a particular focus on the simultaneous inactivation of *M. aeruginosa* and removal of AOM. At low chemical doses (i.e., 300 mg/L La_2CuO_4 and 0.24 mM PMS), the La_2CuO_4/PMS system could remove *M. aeruginosa* cells by 97% and chlorophyll-a by 100% within 20 min. The treatment is superior over the PMS treatment alone at the identical conditions with a 19% removal of algal cells. The resulting sulfate as the final product of added PMS was below the standard of drinking water, which was not a concern in a drinking water treatment scenario. Meanwhile, the catalytic system exhibited an excellent pH adaptability and a reliable treatment performance in realistic natural water matrixes. Besides the treatment performance, underlying catalytic mechanisms in removing algal cells were explored by monitoring of extracellular cell morphology of algae cells, identifying ROS, measuring zeta potential and DFT calculation. $^{\bullet}OH$, $SO_4^{\bullet-}$, $^1O_2$ and $^{\bullet}O_2^-$ were all generated in the La_2CuO_4/PMS system, among which surface-bound $^{\bullet}OH$ and $SO_4^{\bullet-}$ played a key role in the algae inactivation. The heterogeneous catalytic mechanism of simultaneous coagulation and chemical oxidation was proposed, where the La portion in La_2CuO_4 promptly facilitated the destabilization of algae cells and the prompt growth of flocs by lowering the absolute value of zeta potential of algae suspension, while variable Cu portion in La_2CuO_4 facilitated the electron transfer to produce more $^{\bullet}OH$ and $SO_4^{\bullet-}$. Furthermore, the La_2CuO_4/PMS system significantly inhibited the release of toxic MC-LR through chemical degradation rather than physical adsorption, while PMS alone could not directly oxidize the extracellular MC-LR. And the potential degradation pathways of MC-LR in the La_2CuO_4/PMS system were proposed based on the UPLC-MS/MS analysis. Overall, the La_2CuO_4 perovskite activated PMS system provides a promising alternative for the control of cyanobacterial blooms as an emergency measure.

CRediT authorship contribution statement

Panpan Gao: Investigation, Data curation, Writing – original draft. **Yunyi He:** Methodology, Data curation. **Shihuan Lu:** Formal analysis, Resources. **Mengfan He:** Visualization, Formal analysis. **Zhiqun Liu:** Visualization, Formal analysis. **Yang Deng:** Writing – review & editing, Investigation. **Zhiquan Liu:** Writing – review & editing. **Ting Xu:** Formal analysis. **Hangjun Zhang:** Supervision, Writing – review & editing.

Declaration of Competing Interest

The authors declare that they have no known competing financial interests or personal relationships that could have appeared to influence the work reported in this paper.

Data availability

I have shared the link to my data at the attach file step.

Acknowledgments

This work was supported by the Natural Science Foundation of Zhejiang Province (No. LQ22E080003), National Natural Science Foundation of China (No. 42207103), Scientific Research Foundation for Scholars of Hangzhou Normal University (No. 2021QDL061) and Huzhou Bureau of Science and Technology-Special Project for Demonstration Zone of Ecological Civilization (No. 2020ZD2030).

Appendix A. Supporting information

Supplementary data associated with this article can be found in the online version at doi:10.1016/j.apcatb.2023.122511.

References

[1] J. Huisman, G.A. Codd, H.W. Paerl, B.W. Ibelings, J.M.H. Verspagen, P.M. Visser, Cyanobacterial blooms, Nat. Rev. Microbiol. 16 (2018) 471–483, https://doi.org/10.1038/s41579-018-0040-1.
[2] I. Chorus, I.R. Falconer, H.J. Salas, J. Bartram, Health risks caused by freshwater cyanobacteria in recreational waters, J. Toxicol. Environ. Health B 3 (2000) 323–347, https://doi.org/10.1080/109374000436364.
[3] E.C. Wert, F.L. Rosario-Ortiz, Intracellular organic matter from cyanobacteria as a precursor for carbonaceous and nitrogenous disinfection byproducts, Environ. Sci. Technol. 47 (2013) 6332–6340, https://doi.org/10.1021/es400834k.
[4] C.W.K. Chow, M. Drikas, J. House, M.D. Burch, R.M.A. Velzeboer, The impact of conventional water treatment processes on cells of the cyanobacterium *Microcystis aeruginosa*, Water Res. 33 (1999) 3253–3262, https://doi.org/10.1016/S0043-1354(99)00051-2.
[5] V. Montemezzani, I.C. Duggan, I.D. Hogg, R.J. Craggs, Screening of potential zooplankton control technologies for wastewater treatment high rate algal ponds, Algal Res. 22 (2017) 1–13, https://doi.org/10.1016/j.algal.2016.11.022.
[6] R. Sun, P. Sun, J. Zhang, S. Esquivel-Elizondo, Y. Wu, Microorganisms-based methods for harmful algal blooms control: A review, Bioresour. Technol. 248 (2018) 12–20, https://doi.org/10.1016/j.biortech.2017.07.175.
[7] J.R. Laszakovits, A.A. MacKay, Removal of cyanotoxins by potassium permanganate: Incorporating competition from natural water constituents, Water Res. 155 (2019) 86–95, https://doi.org/10.1016/j.watres.2019.02.018.
[8] D.L. Widrig, K.A. Gray, K.S. McAuliffe, Removal of algal-derived organic material by preozonation and coagulation: Monitoring changes in organic quality by pyrolysis-GC-MS, Water Res. 30 (1996) 2621–2632, https://doi.org/10.1016/S0043-1354(96)00162-5.
[9] J. Lee, U. von Gunten, J.H. Kim, Persulfate-based advanced oxidation: Critical assessment of opportunities and roadblocks, Environ. Sci. Technol. 54 (2020) 3064–3081, https://doi.org/10.1021/acs.est.9b07082.
[10] R. Xiao, K. Liu, L. Bai, D. Minakata, Y. Seo, R. Kaya Göktaş, D.D. Dionysiou, C.-J. Tang, Z. Wei, R. Spinney, Inactivation of pathogenic microorganisms by sulfate radical: Present and future, Chem. Eng. J. 371 (2019) 222–232, https://doi.org/10.1016/j.cej.2019.03.296.
[11] W. Wang, H. Wang, G. Li, T. An, H. Zhao, P.K. Wong, Catalyst-free activation of persulfate by visible light for water disinfection: Efficiency and mechanisms, Water Res. 157 (2019) 106–118, https://doi.org/10.1016/j.watres.2019.03.071.
[12] W. Wang, H. Wang, G. Li, P.K. Wong, T. An, Visible light activation of persulfate by magnetic hydrochar for bacterial inactivation: Efficiency, recyclability and mechanisms, Water Res. 176 (2020), 115746, https://doi.org/10.1016/j.watres.2020.115746.
[13] W. Wang, P. Liao, G. Li, H. Chen, J. Cen, S. Lu, P.K. Wong, T. An, Photocatalytic inactivation and destruction of harmful microalgae Karenia mikimotoi under visible-light irradiation: Insights into physiological response and toxicity assessment, Environ. Res. 198 (2021), 111295, https://doi.org/10.1016/j.envres.2021.111295.
[14] M. Kohantorabi, G. Moussavi, S. Giannakis, A review of the innovations in metal- and carbon-based catalysts explored for heterogeneous peroxymonosulfate (PMS) activation, with focus on radical vs. non-radical degradation pathways of organic contaminants, Chem. Eng. J. 411 (2021), 127957, https://doi.org/10.1016/j.cej.2020.127957.
[15] J. Zhou, J. Liu, Z. Zhao, W. Peng, F. Cui, Z. Liang, Microcystis aeruginosa-laden water treatment using peroxymonosulfate enhanced Fe(II) coagulation: Performance and the role of in situ formed Fe_3O_4, Chem. Eng. J. 382 (2020), 123012, https://doi.org/10.1016/j.cej.2019.123012.
[16] Y. Chen, P. Xie, Z. Wang, R. Shang, S. Wang, UV/persulfate preoxidation to improve coagulation efficiency of *Microcystis aeruginosa*, J. Hazard. Mater. 322 (2017) 508–515, https://doi.org/10.1016/j.jhazmat.2016.10.017.
[17] G. Fan, X. Lin, Y. You, B. Du, X. Li, J. Luo, Magnetically separable $ZnFe_2O_4$/Ag_3PO_4/g-C_3N_4 photocatalyst for inactivation of *Microcystis aeruginosa*:

Characterization, performance and mechanism, J. Hazard. Mater. 421 (2022), 126703, https://doi.org/10.1016/j.jhazmat.2021.126703.
[18] G. Fan, B. Du, J. Zhou, Z. Yan, Y. You, J. Luo, Porous self-floating 3D Ag_2O/g-C_3N_4 hydrogel and photocatalytic inactivation of *Microcystis aeruginosa* under visible light, Chem. Eng. J. 404 (2021), https://doi.org/10.1016/j.cej.2020.126509.
[19] K. Wang, C. Han, Z. Shao, J. Qiu, S. Wang, S. Liu, Perovskite oxide catalysts for advanced oxidation reactions, Adv. Funct. Mater. 31 (2021) 2102089, https://doi.org/10.1002/adfm.202102089.
[20] J. Miao, X. Duan, J. Li, J. Dai, B. Liu, S. Wang, W. Zhou, Z. Shao, Boosting performance of lanthanide magnetism perovskite for advanced oxidation through lattice doping with catalytically inert element, Chem. Eng. J. 355 (2019) 721–730, https://doi.org/10.1016/j.cej.2018.08.192.
[21] C. Su, X. Duan, J. Miao, Y. Zhong, W. Zhou, S. Wang, Z. Shao, Mixed conducting perovskite materials as superior catalysts for fast aqueous-phase advanced oxidation: a mechanistic study, ACS Catal. 7 (2016) 388–397, https://doi.org/10.1021/acscatal.6b02303.
[22] H. Zhu, P. Zhang, S. Dai, Recent advances of lanthanum-based perovskite oxides for catalysis, ACS Catal. 5 (2015) 6370–6385, https://doi.org/10.1021/acscatal.5b01667.
[23] P. Gao, S. Yan, X. Tian, Y. Nie, Y. Wang, Y. Deng, J. Tu, Identification and manipulation of active centers on perovskites to enhance catalysis of peroxymonosulfate for degradation of emerging pollutants in water, J. Hazard. Mater. 424 (2022), 127384, https://doi.org/10.1016/j.jhazmat.2021.127384.
[24] P. Gao, X. Tian, W. Fu, Y. Wang, Y. Nie, C. Yang, Y. Deng, Copper in $LaMnO_3$ to promote peroxymonosulfate activation by regulating the reactive oxygen species in sulfamethoxazole degradation, J. Hazard. Mater. 411 (2021), 125163, https://doi.org/10.1016/j.jhazmat.2021.125163.
[25] G. Fan, Z. Chen, Z. Yan, B. Du, H. Pang, D. Tang, J. Luo, J. Lin, Efficient integration of plasmonic Ag/AgCl with perovskite-type $LaFeO_3$: Enhanced visible-light photocatalytic activity for removal of harmful algae, J. Hazard. Mater. 409 (2021), 125018, https://doi.org/10.1016/j.jhazmat.2020.125018.
[26] X. Tian, P. Gao, Y. Nie, C. Yang, Z. Zhou, Y. Li, Y. Wang, A novel singlet oxygen involved peroxymonosulfate activation mechanism for degradation of ofloxacin and phenol in water, Chem. Commun. 53 (2017) 6589–6592, https://doi.org/10.1039/C7CC02820B.
[27] P. Gao, X. Tian, Y. Nie, C. Yang, Z. Zhou, Y. Wang, Promoted peroxymonosulfate activation into singlet oxygen over perovskite for ofloxacin degradation by controlling the oxygen defect concentration, Chem. Eng. J. 359 (2019) 828–839, https://doi.org/10.1016/j.cej.2018.11.184.
[28] A. Shahzad, J. Ali, J. Ifthikar, G.G. Aregay, J. Zhu, Z. Chen, Z. Chen, Non-radical PMS activation by the nanohybrid material with periodic confinement of reduced graphene oxide (rGO) and Cu hydroxides, J. Hazard. Mater. 392 (2020), 122316, https://doi.org/10.1016/j.jhazmat.2020.122316.
[29] M. Sukumar, L.J. Kennedy, J.J. Vijaya, B. Al-Najar, M. Bououdina, Co^{2+} substituted La_2CuO_4/$LaCoO_3$ perovskite nanocomposites: synthesis, properties and heterogeneous catalytic performance, N. J. Chem. 42 (2018) 18128–18142, https://doi.org/10.1039/C8NJ04133D.
[30] Y. Liu, Y. Wei, M. Liu, Y. Bai, G. Liu, X. Wang, S. Shang, W. Gao, C. Du, J. Chen, Y. Liu, Two-dimensional metal-organic framework film for realizing optoelectronic synaptic plasticity, Angew. Chem. Int. Ed. 60 (2021) 17440–17445, https://doi.org/10.1002/anie.202106519.
[31] H. Wang, L. Zhang, C. Hu, X. Wang, L. Lyu, G. Sheng, Enhanced degradation of organic pollutants over Cu-doped $LaAlO_3$ perovskite through heterogeneous Fenton-like reactions, Chem. Eng. J. 332 (2018) 572–581, https://doi.org/10.1016/j.cej.2017.09.058.
[32] C. Cheng, S. Gao, J. Zhu, G. Wang, L. Wang, X. Xia, Enhanced performance of $LaFeO_3$ perovskite for peroxymonosulfate activation through strontium doping towards 2,4-D degradation, Chem. Eng. J. 384 (2020), 123377, https://doi.org/10.1016/j.cej.2019.123377.
[33] H. Chen, Y. Xu, K. Zhu, H. Zhang, Understanding oxygen-deficient $La_2CuO_{4-\delta}$ perovskite activated peroxymonosulfate for bisphenol A degradation: The role of localized electron within oxygen vacancy, Appl. Catal. B: Environ. 284 (2021), 119732, https://doi.org/10.1016/j.apcatb.2020.119732.
[34] X. Wang, J. Li, K. Chen, J. Li, Y. Jia, Q. Mei, Q. Wang, Facile synthesis of oxygen vacancies enriched $ZnFe_2O_4$ for effective photocatalytic peroxodisulfate activation, Sep. Purif. Technol. 303 (2022), 122205, https://doi.org/10.1016/j.seppur.2022.122205.
[35] Z. Chen, J. Li, M. Chen, K.Y. Koh, Z. Du, K.Y.-H. Gin, Y. He, C.N. Ong, J.P. Chen, *Microcystis aeruginosa* removal by peroxides of hydrogen peroxide, peroxymonosulfate and peroxydisulfate without additional activators, Water Res. (2021), 117263, https://doi.org/10.1016/j.watres.2021.117263.
[36] J. Qi, H. Lan, R. Liu, H. Liu, J. Qu, Efficient *Microcystis aeruginosa* removal by moderate photocatalysis-enhanced coagulation with magnetic Zn-doped Fe_3O_4 particles, Water Res. 171 (2020), 115448, https://doi.org/10.1016/j.watres.2019.115448.
[37] X. Chen, D. Vione, T. Borch, J. Wang, Y. Gao, Nano-MoO_2 activates peroxymonosulfate for the degradation of PAH derivatives, Water Res. 192 (2021), 116834, https://doi.org/10.1016/j.watres.2021.116834.
[38] F. Chen, X.-L. Wu, L. Yang, C. Chen, H. Lin, J. Chen, Efficient degradation and mineralization of antibiotics via heterogeneous activation of peroxymonosulfate by using graphene supported single-atom Cu catalyst, Chem. Eng. J. 394 (2020), 124904, https://doi.org/10.1016/j.cej.2020.124904.
[39] E.C. Wert, M.M. Dong, F.L. Rosario-Ortiz, Using digital flow cytometry to assess the degradation of three cyanobacteria species after oxidation processes, Water Res. 47 (2013) 3752–3761, https://doi.org/10.1016/j.watres.2013.04.038.
[40] P. Jia, Y. Zhou, X. Zhang, Y. Zhang, R. Dai, Cyanobacterium removal and control of algal organic matter (AOM) release by UV/H_2O_2 pre-oxidation enhanced Fe(II) coagulation, Water Res. 131 (2018) 122–130, https://doi.org/10.1016/j.watres.2017.12.020.
[41] B. Wang, Y. Zhang, Y. Qin, H. Li, Removal of *Microcystis aeruginosa* and control of algal organic matter by Fe(II)/peroxymonosulfate pre-oxidation enhanced coagulation, Chem. Eng. J. 403 (2021), 126381, https://doi.org/10.1016/j.cej.2020.126381.
[42] J. Xu, X. Zheng, Z. Feng, Z. Lu, Z. Zhang, W. Huang, Y. Li, D. Vuckovic, Y. Li, S. Dai, G. Chen, K. Wang, H. Wang, J.K. Chen, W. Mitch, Y. Cui, Organic wastewater treatment by a single-atom catalyst and electrolytically produced H_2O_2, Nat. Sustain. 4 (2020) 233–241, https://doi.org/10.1038/s41893-020-00635-w.
[43] R.K. Henderson, A. Baker, S.A. Parsons, B. Jefferson, Characterisation of algogenic organic matter extracted from cyanobacteria, green algae and diatoms, Water Res. 42 (2008) 3435–3445, https://doi.org/10.1016/j.watres.2007.10.032.
[44] F. Qu, H. Liang, J. He, J. Ma, Z. Wang, H. Yu, G. Li, Characterization of dissolved extracellular organic matter (dEOM) and bound extracellular organic matter (bEOM) of *Microcystis aeruginosa* and their impacts on UF membrane fouling, Water Res. 46 (2012) 2881–2890, https://doi.org/10.1016/j.watres.2012.02.045.
[45] X. Zheng, X. Niu, D. Zhang, X. Ye, J. Ma, M. Lv, Z. Lin, Removal of *Microcystis aeruginosa* by natural pyrite-activated persulfate: Performance and the significance of iron species, Chem. Eng. J. 428 (2022), 132565, https://doi.org/10.1016/j.cej.2021.132565.
[46] G.V. Buxton, C.L. Greenstock, W.P. Helman, A.B. Ross, Critical review of rate constants for reactions of hydrated electrons, hydrogen atoms and hydroxyl radicals (•OH/•O^- in aqueous solution, J. Phys. Chem. Ref. Data 17 (1988) 513–886, https://doi.org/10.1063/1.555805.
[47] P. Neta, R.E. Huie, A.B. Ross, Rate constants for reactions of inorganic radicals in aqueous solution, J. Phys. Chem. Ref. Data 17 (1988) 1027–1284, https://doi.org/10.1063/1.555808.
[48] Y. Wang, H. Sun, H.M. Ang, M.O. Tadé, S. Wang, 3D-hierarchically structured MnO_2 for catalytic oxidation of phenol solutions by activation of peroxymonosulfate: Structure dependence and mechanism, Appl. Catal. B: Environ. 164 (2015) 159–167, https://doi.org/10.1016/j.apcatb.2014.09.004.
[49] X. Wang, Z. Liu, X. Shi, Y. Jia, G. Zhu, J. Peng, Q. Wang, Optical and photocatalytic characteristics of Se-doped h-boron nitride: Experimental assessments and DFT calculations, J. Alloy. Compd. 909 (2022), 164791, https://doi.org/10.1016/j.jallcom.2022.164791.
[50] M. Zalibera, P. Rapta, A. Staško, L. Brindzová, V. Brezová, Thermal generation of stable spin trap adducts with super-hyperfine structure in their EPR spectra: An alternative EPR spin trapping assay for radical scavenging capacity determination in dimethylsulphoxide, Free Radic. Res. 43 (2009) 457–469, https://doi.org/10.1080/10715760902846140.
[51] B. Li, W. Wang, J. Zhao, Z. Wang, B. Su, Y. Hou, Z. Ding, W.-J. Ong, S. Wang, All-solid-state direct Z-scheme $NiTiO_3$/$Cd_{0.5}Zn_{0.5}S$ heterostructures for photocatalytic hydrogen evolution with visible light, J. Mater. Chem. A 9 (2021) 10270–10276, https://doi.org/10.1039/D1TA01220G.
[52] B. Su, H. Huang, Z. Ding, M.B.J. Roeffaers, S. Wang, J. Long, S-scheme $CoTiO_3$/$Cd_{9.51}Zn_{0.49}S_{10}$ heterostructures for visible-light driven photocatalytic CO_2 reduction, J. Mater. Sci. Technol. 124 (2022) 164–170, https://doi.org/10.1016/j.jmst.2022.01.030.
[53] J. Hu, H. Dong, J. Qu, Z. Qiang, Enhanced degradation of iopamidol by peroxymonosulfate catalyzed by two pipe corrosion products (CuO and delta-MnO_2), Water Res. 112 (2017) 1–8, https://doi.org/10.1016/j.watres.2017.01.025.
[54] L. Wang, H. Xu, N. Jiang, Z. Wang, J. Jiang, T. Zhang, Trace cupric species triggered decomposition of peroxymonosulfate and degradation of organic pollutants: Cu(III) being the primary and selective intermediate oxidant, Environ. Sci. Technol. 54 (2020) 4686–4694, https://doi.org/10.1021/acs.est.0c00284.
[55] W.D. Oh, S.K. Lua, Z. Dong, T.T. Lim, Performance of magnetic activated carbon composite as peroxymonosulfate activator and regenerable adsorbent via sulfate radical-mediated oxidation processes, J. Hazard. Mater. 284 (2015) 1–9, https://doi.org/10.1016/j.jhazmat.2014.10.042.
[56] J. Wang, C. Wang, H. Guo, T. Ye, Y. Liu, X. Cheng, W. Li, B. Yang, E. Du, Crucial roles of oxygen and superoxide radical in bisulfite-activated persulfate oxidation of bisphenol AF: Mechanisms, kinetics and DFT studies, J. Hazard. Mater. 391 (2020), 122228, https://doi.org/10.1016/j.jhazmat.2020.122228.
[57] G.-D. Fang, D.D. Dionysiou, S.R. Al-Abed, D.-M. Zhou, Superoxide radical driving the activation of persulfate by magnetite nanoparticles: Implications for the degradation of PCBs, Appl. Catal. B: Environ. 129 (2013) 325–332, https://doi.org/10.1016/j.apcatb.2012.09.042.
[58] M. Li, C. Liu, Z. Zhang, S. Cao, H. Liu, S. Shen, W. Wang, Ultrathin Cu-Fe oxide nanosheets boosting persulfate activation to remove organic pollutants with coupling and transformation between radical and nonradical mechanism, Sep. Purif. Technol. 281 (2022), https://doi.org/10.1016/j.seppur.2021.119978.
[59] X. Sun, D. Xu, P. Dai, X. Liu, F. Tan, Q. Guo, Efficient degradation of methyl orange in water via both radical and non-radical pathways using Fe-Co bimetal-doped MCM-41 as peroxymonosulfate activator, Chem. Eng. J. 402 (2020), 125881, https://doi.org/10.1016/j.cej.2020.125881.
[60] Q. Zhou, L. Chen, L. Yan, T. Cheng, X. Wang, Y. Zhang, Singlet oxygen-dominated transformation of oxytetracycline by peroxymonosulfate with CoAl-LDH modified hierarchical porous ceramics: Toxicity assessment, Chem. Eng. J. 436 (2022), 135199, https://doi.org/10.1016/j.cej.2022.135199.
[61] H. Li, C. Shan, B. Pan, Fe (III)-doped g-C_3N_4 mediated peroxymonosulfate activation for selective degradation of phenolic compounds via high-valent iron-

oxo species, Environ. Sci. Technol. 52 (2018) 2197–2205, https://doi.org/10.1021/acs.est.7b05563.
[62] X. Yang, L. Yao, Y. Wang, X. Zhang, P. Ren, Simultaneous removal of algae, microcystins and disinfection byproduct precursors by peroxymonosulfate (PMS)-enhanced Fe(III) coagulation, Chem. Eng. J. 445 (2022), https://doi.org/10.1016/j.cej.2022.136689.
[63] X. He, A. Wang, P. Wu, S. Tang, Y. Zhang, L. Li, P. Ding, Photocatalytic degradation of microcystin-LR by modified TiO_2 photocatalysis: A review, Sci. Total Environ. 743 (2020), 140694, https://doi.org/10.1016/j.scitotenv.2020.140694.
[64] W. Jiang, L. Chen, S.R. Batchu, P.R. Gardinali, L. Jasa, B. Marsalek, R. Zboril, D. D. Dionysiou, K.E. O'Shea, V.K. Sharma, Oxidation of microcystin-LR by ferrate (VI): kinetics, degradation pathways, and toxicity assessments, Environ. Sci. Technol. 48 (2014) 12164–12172, https://doi.org/10.1021/es5030355.
[65] W.-D. Oh, Z. Dong, T.-T. Lim, Generation of sulfate radical through heterogeneous catalysis for organic contaminants removal: current development, challenges and prospects, Appl. Catal. B: Environ. 194 (2016) 169–201, https://doi.org/10.1016/j.apcatb.2016.04.003.
[66] T. Fotiou, T.M. Triantis, T. Kaloudis, L.M. Pastrana-Martínez, V. Likodimos, P. Falaras, A.M.T. Silva, A. Hiskia, Photocatalytic degradation of microcystin-LR and off-odor compounds in water under UV-A and solar light with a nanostructured photocatalyst based on reduced graphene oxide–TiO_2 composite. Identification of intermediate products, Ind. Eng. Chem. Res. 52 (2013) 13991–14000, https://doi.org/10.1021/ie400382r.
[67] M. Nawaz, M. Moztahida, J. Kim, A. Shahzad, J. Jang, W. Miran, D.S. Lee, Photodegradation of microcystin-LR using graphene-TiO_2/sodium alginate aerogels, Carbohydr. Polym. 199 (2018) 109–118, https://doi.org/10.1016/j.carbpol.2018.07.007.
[68] X. Hu, X. Hu, C. Tang, S. Wen, X. Wu, J. Long, X. Yang, H. Wang, L. Zhou, Mechanisms underlying degradation pathways of microcystin-LR with doped TiO_2 photocatalysis, Chem. Eng. J. 330 (2017) 355–371, https://doi.org/10.1016/j.cej.2017.07.161.
[69] M. Zhou, J. Chen, S. Yu, B. Chen, C. Chen, L. Shen, B. Li, H. Lin, The coupling of persulfate activation and membrane separation for the effective pollutant degradation and membrane fouling alleviation, Chem. Eng. J. 451 (2023), 139009, https://doi.org/10.1016/j.cej.2022.139009.
[70] J. Zhou, J. Liu, Z. Zhao, W. Peng, F. Cui, Z. Liang, Microcystis aeruginosa-laden water treatment using peroxymonosulfate enhanced Fe(II) coagulation: Performance and the role of in situ formed Fe_3O_4, Chem. Eng. J. 382 (2020), 123012, https://doi.org/10.1016/j.cej.2019.123012.
[71] N. Gu, Y. Wu, J. Gao, X. Meng, P. Zhao, H. Qin, K. Wang, *Microcystis aeruginosa* removal by in situ chemical oxidation using persulfate activated by Fe^{2+} ions, Ecol. Eng. 99 (2017) 290–297, https://doi.org/10.1016/j.ecoleng.2016.11.048.
[72] Z. Yang, J. Hou, Z. Pan, M. Wu, M. Zhang, J. Wu, L. Miao, A innovative stepwise strategy using magnetic Fe_3O_4-co-graft tannin/polyethyleneimine composites in a coupled process of sulfate radical-advanced oxidation processes to control harmful algal blooms, J. Hazard. Mater. 439 (2022), 129485, https://doi.org/10.1016/j.jhazmat.2022.129485.
[73] B. Yu, X. Li, M. He, Y. Li, J. Ding, Y. Zhong, H. Zhang, Selective production of singlet oxygen for harmful cyanobacteria inactivation and cyanotoxins degradation: Efficiency and mechanisms, J. Hazard. Mater. 441 (2023), 129940, https://doi.org/10.1016/j.jhazmat.2022.129940.
[74] H. Zhang, B. Yu, X. Li, Y. Li, Y. Zhong, J. Ding, Inactivation of *Microcystis aeruginosa* by peroxydisulfate activated with single-atomic iron catalysis: Efficiency and mechanisms, J. Environ. Chem. Eng. 10 (2022), 108310, https://doi.org/10.1016/j.jece.2022.108310.